A CONFOCAL FABRY-PEROT INTERFEROMETER FOR USE IN LIDAR RECEIVERS

by

Kerry Ann Neal

A thesis submitted in partial fulfillment
of the requirements for the degree

of

Master of Science

in

Electrical Engineering

MONTANA STATE UNIVERSITY
Bozeman, Montana

November, 2009

APPROVAL

of a thesis submitted by

Kerry Ann Neal

This thesis has been read by each member of the thesis committee and has been found to be satisfactory regarding content, English usage, format, citations, bibliographic style, and consistency, and is ready for submission to the Division of Graduate Education.

Dr. Kevin S. Repasky

Approved for the Department of Electrical Engineering

Dr. Robert Maher

Approved for the Division of Graduate Education

Dr. Carl Fox

STATEMENT OF PERMISSION TO USE

In presenting this thesis in partial fulfullment of the requirements for a master's degree at Montana State University, I agree that the Library shall make it available to borrowers under rules of the Library.

If I have indicated my intention to copyright this thesis by including a copyright notice page, copying is allowable only for scholarly purposes, consistent with "fair use" as prescribed in the U.S. Copyright Law. Requests for permission for extend quotation from or reproduction of this thesis in whole or in parts may be granted only by the copyright holder.

Kerry Ann Neal

November, 2009

ACKNOWLEDGEMENTS

I would foremost like to thank my advisor Kevin Repasky for taking me on this project and providing a vast amount of insight, patience, and guidance. I would like to thank John Carlsten for originally devising this project, as well as his boundless knowledge and enthusiasm of all things optics. Thanks to Cale Gentry, a summer intern with the Research Experience for Undergraduates (REU), who took data with the 1 cm cavity that is presented in this thesis.

I would also like to thank Ira Glass of NPR for keeping me company in the dark, quiet lab while I ran experiments. I would especially like to acknowledge my family and friends for all of their support throughout this endeavour, especially when I was frustrated. And finally, to the PCT for motivating me to finish everything in a timely manner.

This work was supported by the NASA EPSCoR grant number NNX08AT69A and a fellowship from the Montana Space Grant Consortium.

TABLE OF CONTENTS

LIST OF TABLES

LIST OF FIGURES

LIST OF FIGURES – CONTINUED

LIST OF FIGURES – CONTINUED

ABSTRACT

A Confoal Fabry-Perot (CFP) interferometer was modeled, designed, built, and characterized. The proposed use of the CFP is as a narrowband filter in the receiver of lidar (light detection and ranging) instruments. Currently, a CFP very similar to the one discussed herein is being used in the High Spectral Resolution Lidar (HSRL), but through this work, the CFP will be adaptable to any lidar receiver. The goal was to characterize the CFP for a variety of parameter spaces that would be of interest to those using the CFP in a lidar receiver. These parameters include how the CFP performs with large diameter multi-spatial mode beams, large off-axis incoming angles, and large waist sizes at the center of the CFP. The modeling revealed that spherical mirrors would be suitable for the experiment. The modeling also demonstrated that angles up to 100 mrad are accepted into the CFP and waist sizes of at least 200 μm in the center of the CFP are useable. The characterization of the CFP was achieved with two experiments. The quality of performance of the CFP was expressed through measurements of finesse and transmission through the CFP for each parameter tested. The results of the experiments showed that the CFP performs optimally when nominally mode-matched or when collimated light is sent into the CFP. Also, the finesse of the CFP drops substantially as a function of the incoming waist size at first and then levels off at a fairly high finesse of around 100, which is a result that deviates from theory.

1

INTRODUCTION

While the Flat-Plate Fabry-Perot (FPFP) interferometer has found its way into a plethora of systems and instruments, the Confocal Fabry Perot (CFP) interferometer, which has several advantages over the FPFP interferometer, has remained largely unnoticed by most of the scientific community. The predominant use of the CFP is in the realm of spectroscopic applications [1]. The first use of the CFP was to study resonance lines in the spectra of elements [1]. Continuing in this vein, current applications of the CFP are to use the interferometer as a way to place variably, close spaced frequency markers to find closely spaced absorption lines of isotopes [2]. The CFP, also known as the spherical or Connes Fabry-Perot, has been in use since the late 1950s, with the first use of the interferometer by Connes [3]. The emergence of the CFP around the invention of the laser is not coincidental. The CFP is useful as a resonator for a laser, and is also well suited to spectrally characterize lasers [4]. Recently, the CFP has been used as a sub-picometer spectral filter for imaging line profiles from the sun because of its high resolution imaging capabilities [5]. This group drew attention to the fact that there is unknown potential of the CFP in most of the scientific community.

The defining characteristic of a CFP is that the two spherical mirrors have equal radii of curvature and are spaced a distance equal to their common radius of curvature. The optical axis of the CFP runs through the center of the mirrors. The focus of both of the mirrors is at the center of the CFP. These features are shown in Figure 1. The path taken through the CFP is such that the light always comes to a focus in the close vicinity of the foci of the mirrors. The deviations from the foci are due to wavefront aberrations. After four passes through the CFP, the light comes back on itself to interfere with each successive roundtrip. The resonant light is transmitted

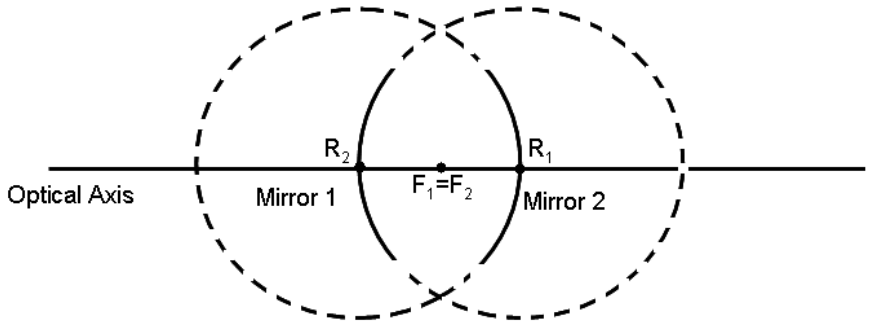

Figure 1: The CFP demonstrates circular symmetry around the optical axis. The radius of curvature of each mirror lies at the center of the opposite mirror and the two mirrors are spaced a distance equal to the radius of curvature. The foci of the mirrors lie in the middle of the CFP.

at the second mirror. Figure 2 in the Theory section shows the four passes through the CFP.

This thesis describes the development of a CFP as a narrowband filter, which allows for large incoming angles of light into the cavity and large waist sizes at the center of the cavity. The properties of the CFP design are utilized for the purposes proposed and the ideal configurations of the CFP are sought. The first use of the CFP is in the High Spectral Resolution Lidar (HSRL), also being built at Montana State University. The basic concept of lidar (light detection and ranging) is to send laser light out to a target, the atmosphere in this case, and the light which is scattered off particulates in the atmosphere is collected by a telescope and sent into the receiver of the instrument. The CFP is used in the receiver of the HSRL. The CFP resonance is locked to the laser and used to pass the desired signal from the atmosphere through the filter. In the case of the HSRL, the backscattered signal from the atmosphere consists of molecular and aerosol information. The CFP is used to distinguish between the two. The aerosol return is the desired signal and also possesses a narrower linewidth

than the molecular signal. The linewidth of the CFP is designed to coincide with the linewidth of the signal from the aerosols.

The most basic of filters to use in a lidar receiver are interference filters that can be obtained from a commercial manufacturer. These filters can achieve a bandwidth of about 1 nm [6]. The interference filters operate on the same principles as the FPFP interferometers on a very small scale. The filter has a dielectric where the air gap is generally in a Fabry-Perot. On either side of the dielectric are coatings. Usually an interference filter is composed of several layers of these Fabry-Perot cavities [6]. A large disadvantage of the interference filter is that light at any angle will tune the filter such that the light passed is not filtered at the wavelength the filter was built to pass. Also, interference filters do not have the precision required by many lidars, which can be achieved by using other methods of filtering. Typically lidar systems will use interference filters in combination with another form of filter such as a FPFP etalon [7], [8]. Many lidar instruments presently use only FPFP interferometers [9], which have the disadvantage of being difficult to align and sensitive to incoming angles [10]. Both of these issues do not exist with the CFP. Another form of filtering the signal is to use an atomic and molecular absorption filter [11]. While this type of filter will accept large angles, it is often inconvenient to find a laser at the wavelength of the absorption and the filters operate under high maintenance conditions [10].

While the CFP is currently a novel approach to filtering light in the receiver of a lidar system, this technique will hopefully become useful in a plethora of lidar systems. There are several advantages of the CFP over a FPFP and other methods of filtering the scattered light. The intent herein is to characterize the CFP such that parameters necessary for other systems have already been explored here and can easily be adjusted for the needs of other lidar systems.

The thesis is organized into five parts. The next chapter explains the theory of the CFP and highlights several advantages of the CFP over the FPFP. Modeling of the CFP is then addressed. As a precursor to beginning the experiment, there were several aspects that needed to be determined first, such as which conic mirrors to use, as well as an estimate of preliminary boundaries of parameters the CFP would accept. The experiment section discusses the design and the building of the CFP, as well as the two experiments conducted to characterize the CFP. The results of the experiments are discussed in the penultimate chapter, including a comparison of the results to the model and the theory. The final chapter includes a brief summary of the project, as well as remarks on future work.

THEORY

The performance of the CFP is determined by the finesse and the transmission through the CFP. A thorough understanding of these concepts is developed, as well as how they pertain to the CFP. Other considerations are a basic discussion of the CFP as an interferometer. The more complicated mode structure of the multimode beams and how they are expected to perform theoretically in the CFP is also addressed.

The path an optical ray follows through the CFP is shown in Figure 2. The incident light transmitted through the first mirror travels to the second mirror. This light is reflected from the second mirror, passing through the focal point of the second mirror back to the first mirror. The light is reflected off of the first mirror to the second mirror, where the light is again reflected and passes through the focal point to the first mirror, completing the round trip. The resonance condition occurs when the internal path length of the CFP is equal to an integer number of wavelengths corresponding to the light traveling through the cavity, resulting in constructive interference after each round trip. The relative frequency difference between adjacent cavity resonances is called the Free Spectral Range (FSR) and is given as:

$$FSR = \frac{c}{4L}, \tag{1}$$

where c is the speed of light and L is the cavity length. The FSR for a FPFP is a factor of two larger than the FSR for the CFP, and is given as, FSR=c/2L. The reason for the reduction of the FSR in the CFP by a factor of two is the extra two passes through the cavity.

A second important parameter describing the performance of the CFP is the finesse. The finesse is related to the frequency resolution of the CFP and is defined

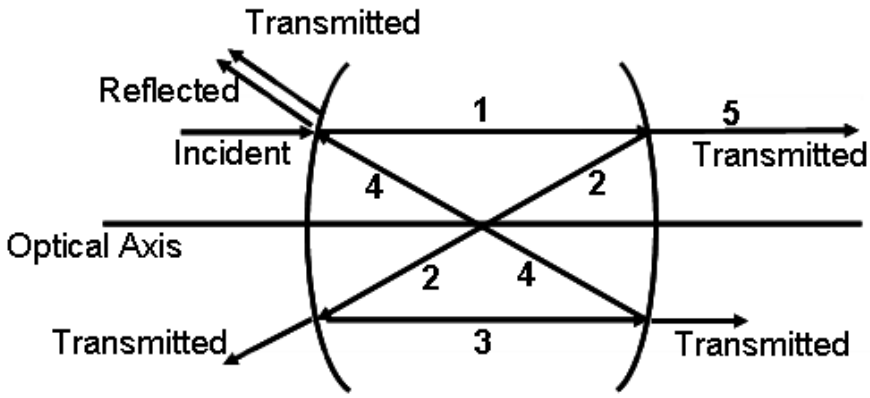

Figure 2: The path of light through the CFP.

as the FSR divided by the full-width half-maximum (FWHM) of the resonant peak.

$$\mathcal{F} = \frac{FSR}{FWHM}, \tag{2}$$

The FSR and FWHM are shown in Figure 3. The FSR shown in Figure 3a. is shown as displayed on the oscilloscope. The CFP is driven by a ramp generator that applies a voltage to the CFP and scans through a FSR. The time axis is representative of the frequency difference between adjacent resonances. For the case shown below, the CFP is 5 cm in length, and the frequency represented between resonances on the x-axis is therefore 1.5 GHz. The FSR is fixed by the length of the cavity. The finesse is related to the number of passes the light makes within the CFP, which is directly related to the reflectivity of the CFP mirrors. A factor that decreases the finesse of the CFP is the spherical aberration which is an inherent characteristic of spherical mirrors. Spherical aberration is a fourth-order wavefront effect [12]. The effect of spherical aberration is that the rays do not focus to one spot, but rather focus in a region where there are small deviations from each ray's focus. The spread of the focus region is due to the radius of curvature of the mirrors. If the mirror has a short focal length, the bending of the rays towards the focus is more extreme, and the spread

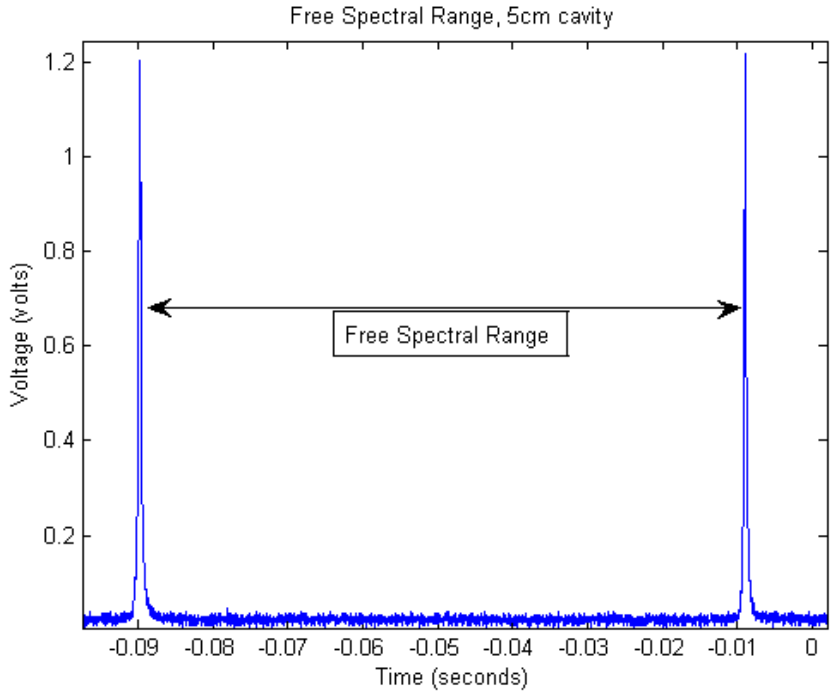

a.

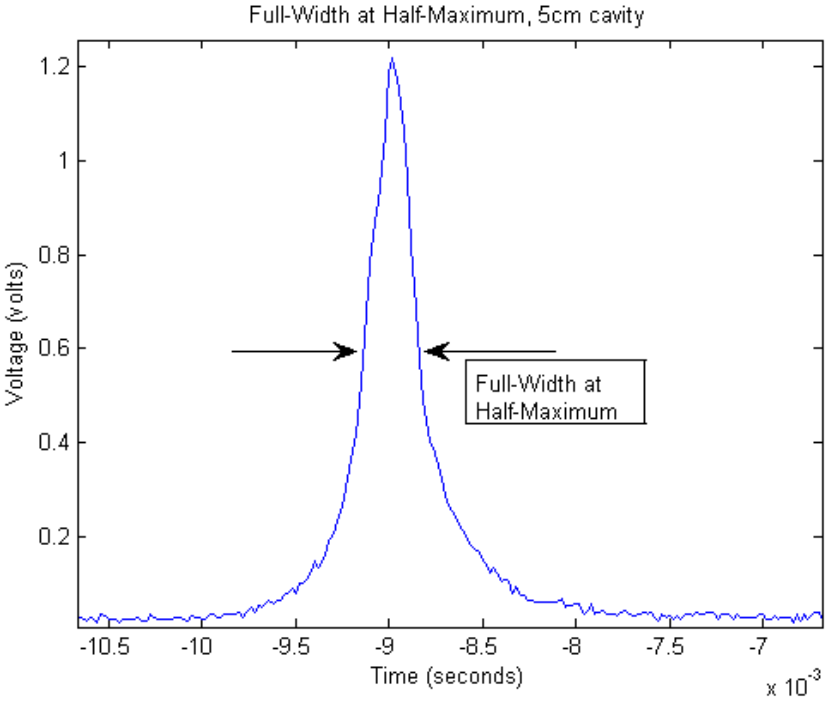

b.

Figure 3: An example of a free spectral range is displayed in (a), while the full-width at half-maximum is displayed in (b).

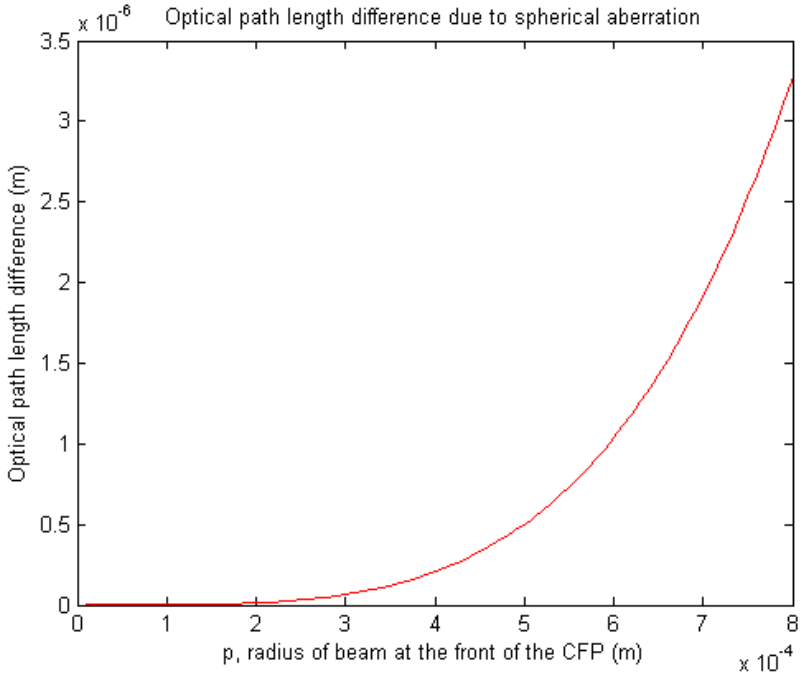

Figure 4: The optical path length difference as a function of the radius of the incoming beam through the CFP due to the effect of spherical aberration.

of the focal points is greater, enhancing the spherical aberration effect [12]. If the radius of curvature is much larger than the diameter of the mirrors, the spherical mirror aberration effect is less. The optical path length difference due to spherical aberration can be expressed as [13]:

$$\Delta = \frac{\rho^4}{R_c^3}, \tag{3}$$

where ρ is the distance off-axis from which the light hits each mirror, and R_c is the radius of curvature of the mirrors, which can also be the length between the two mirrors if the configuration of the CFP is confocal. The optical path length difference as a function of the beam radius in the front mirror of the CFP is shown in Figure 4.

The effect of the spherical aberration on the finesse is developed. The total finesse can be thought of as the finesse due to the reflectivities of the mirrors and the

degradation of finesse due to the spherical aberration of the mirrors. The two can be added in quadrature, which is the accepted way to add finesse quantities together and results in the proper scaling of the finesse [14]:

$$\frac{1}{{\mathcal{F}_{tot}}^2} = \frac{1}{\mathcal{F}_{ref}^2} + \frac{1}{\mathcal{F}_{sph}^2}, \tag{4}$$

where $\mathcal{F}_{tot}$ is the total finesse, $\mathcal{F}_{ref}$ is the finesse due to the reflectivity of the mirrors, defined below in Equation 5, and $\mathcal{F}_{sph}$ is the finesse due to the spherical aberration which is a function of the incoming beam radius and the curvature of the mirrors of the CFP.

The finesse due to the reflectivity of the mirrors can be expressed in terms of the reflectivities as [1]:

$$\mathcal{F}_{ref} = \frac{\pi R}{1 - R^2}, \tag{5}$$

where R is the reflectivity of the mirror. The $\mathcal{F}_{ref}$ represents the finesse for the mirrors in the confocal configuration, for any other configuration take the square root of the reflectivity, R.

The finesse due to spherical aberration, $\mathcal{F}_{sph}$, can be developed in an analogous way to the flatness finesse. The flatness finesse, $\mathcal{F}_{flat}$, is well known and used throughout the scientific community [15], [16]. The flatness finesse can be developed in such a way that the finesse from spherical aberration can be derived by analogy. The flatness of a mirror is given by [15]:

$$flatness = \frac{\lambda}{M}, \tag{6}$$

where M is an integer representing the deviation in wavelengths over the surface of the mirror and λ is the wavelength of the incoming light to the cavity. The flatness finesse, $\mathcal{F}_{flat}$, is defined as [15]:

$$\mathcal{F}_{flat} = \frac{M}{2}. \tag{7}$$

The flatness finesse can further be manipulated:

$$\mathcal{F}_{flat} = \frac{M}{2} = \frac{M/\lambda}{2/\lambda} = \frac{\lambda/2}{\lambda/M} = \frac{FSR}{FWHM}. \tag{8}$$

The flatness finesse is the FSR, $\lambda/2$, divided by the flatness of the mirror, λ/M. The analogous quantity of deviation per surface, or FWHM, due to the effect of spherical aberration is given as:

$$FWHM_{sph} = \frac{\rho^4}{4R_c^3}, \tag{9}$$

which is Equation 3 representing the optical path length difference, with an extra factor of four in the denominator, which refers to the optical path length difference per surface of the cavity. Substituting in the values for the FSR and the FWHM for the spherical aberration, the finesse due to spherical aberration can now be represented as:

$$\mathcal{F}_{sph} = \frac{\lambda/2}{\rho^4/4R_c^3}. \tag{10}$$

Upon substituting the expressions for the finesse due to the reflectivity of the mirrors and the finesse due to spherical aberration, the total finesse becomes [14]:

$$\mathcal{F}_{tot} = [(\frac{1-R^2}{\pi R})^2 + (\frac{\rho^4}{2\lambda R_c^3})^2]^{-1/2} \tag{11}$$

The plot of this expression of finesse is shown in Figure 5. There are some crucial assumptions that go into this equation that make it an overestimate of the effect of spherical aberration on the finesse. The first assumption is that the radius of the beam matches the radius of the mirrors, but in actuality, the beam only takes up a small portion of the radius of the mirrors. If the beam radius is much smaller than the radius of the mirrors, then the spherical aberration will be limited [13]. The second approximation is that the beam is collimated and the rays focus to an infinitesimally small bundle [14]. In the experiments presented here, the light never focuses into a small spot. The multimode structure of the beam creates a large spot at the focus.

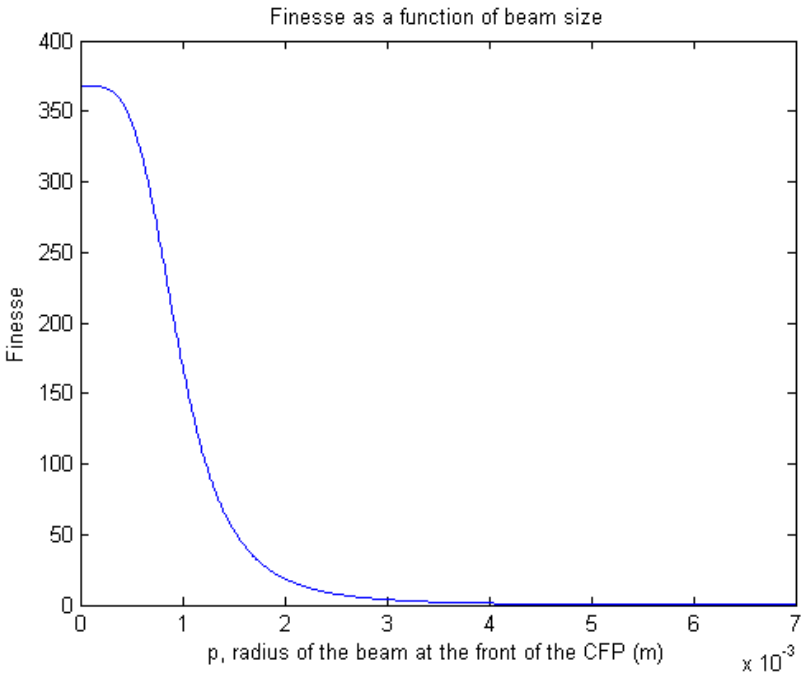

Figure 5: The decrease in finesse as a function of beam radius due to spherical aberration. This plot represents a theoretical prediction of spherical aberration.

Theoretically, considering the above assumptions in determining spherical aberration, the finesse drops to zero fairly quickly, as depicted in Figure 5, this is not expected to be the case experimentally.

The amount of light reflected and transmitted through a CFP, as well as how much is lost due to absorption and scattering, are important parameters for characterization of the CFP. The transmitted and reflected light for a CFP can be calculated in a similar manner as that of a FPFP cavity. The transmission and reflection for a FPFP cavity can be found by considering Figure 6, which shows the accumulated phase for successive passes through the FPFP cavity.

The transmitted light is calculated by adding up all of the light that is transmitted through mirror 2 on the far right side of Figure 6:

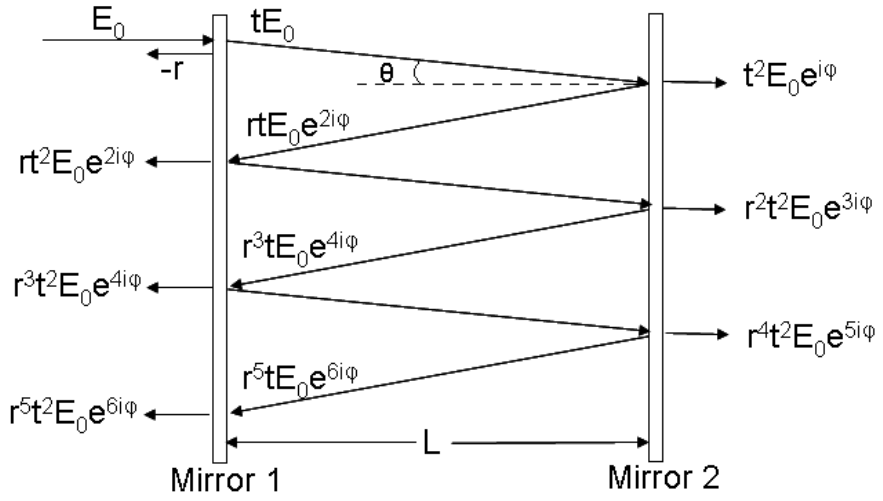

Figure 6: The reflection, transmission, and phase as the incoming light from the top left of the figure bounces in the FPFP cavity. The left side represents the reflected light, the right side represents the transmitted light, and the center of the CFP represents the light maintained within the CFP.

$$E_t = E_0 t^2 e^{i\phi}(1 + r^2 e^{2i\phi} + r^4 e^{4i\phi} + ...). \tag{12}$$

The variable ϕ represents the optical delay for each reflection within the cavity and can be defined as [1]:

$$\phi = \frac{2\pi(L/cos\theta)}{\lambda}, \tag{13}$$

where L is the distance between the two mirrors, λ is the wavelength of the light, and θ is the angle between the ray and the perpendicular to the mirror.

In performing the infinite sum in equation 12, it simplifies to:

$$E_t = \frac{E_0 t^2 e^{i\phi}}{1 - r^2 e^{i\phi}}. \tag{14}$$

The coefficient, R, is the intensity reflection coefficient, which is equal to r^2, where r is the field reflection coefficient. Likewise, the transmission coefficient, T, is equal to

t^2, where t is the field transmission coefficient. Equation 14 can now be written as:

$$E_T = \frac{E_0 T e^{i\phi}}{1 - Re^{i\phi}}. \tag{15}$$

To turn equation 15 into an intensity, E_T is multiplied by its complex conjugate, as $E_T E_T^* \propto I_T$, where I_T is the transmitted intensity. Using this result, equation 15 becomes:

$$I_T = \frac{I_0 T^2}{1 + R^2 - 2Rcos\phi}, \tag{16}$$

where I_0 is the incident intensity. The intensity of the reflection of the beam is found in the same manner, with the result being:

$$I_R = \frac{R(2 - 2cos\phi)}{1 + R^2 - 2Rcos\phi}. \tag{17}$$

For the CFP, the light travels four times through the CFP before the light is transmitted on the right side, as shown in Figure 7. The first transmitted light through the CFP is represented as t^2r^4, neglecting phase, thus the reflection and transmission intensity coefficients will have an extra factor of R^2, or r^4. Other than the extra R^2, the considerations of the CFP and the FPFP cavity are the same.

The CFP is more advantageous than the FPFP for a number of reasons. The CFP is easier to align and is less sensitive to small changes in the orientation of the CFP than the FPFP [1]. Furthermore, the CFP can accept multiple spatial modes, which will all be resonant at the same cavity length, L.

Mode-Matching and Gaussian Beam Approximation

At first approximation, a Gaussian beam can be used to describe how light interacts with the CFP. By matching the phase front of the incoming beam to the curvature of the mirrors, the CFP will be mode-matched, yielding a symmetric transmission

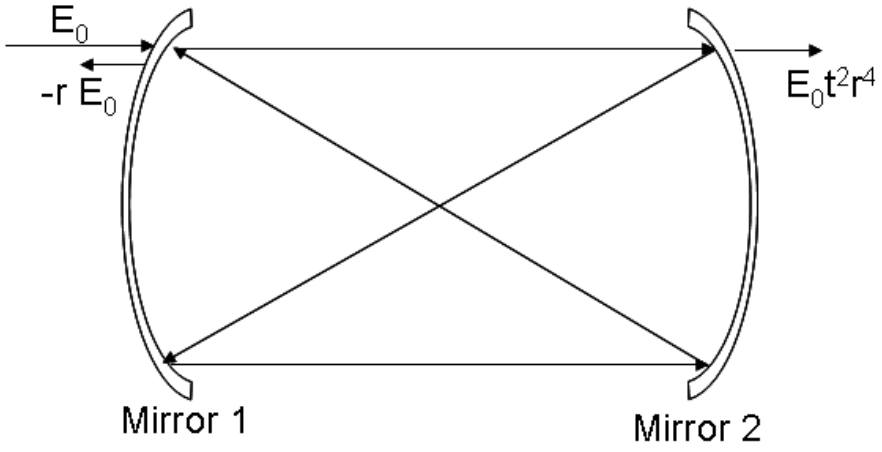

Figure 7: The reflection and transmission through a CFP is shown. The light is not transmitted until four passes have been made through the CFP.

peak [17]. This process is known as mode-matching. To determine the mode-matched condition, certain parameters of the cavity must be calculated for a Gaussian beam.

The Rayleigh range, z_0, is the distance from the beam waist, w_0, to where the beam waist is increased by a factor of $\sqrt{2}$ and is defined as a function of the radius of curvature of the mirrors, R_m, and the distance between the two mirrors, L,

$$z_0 = \frac{1}{2}\sqrt{L(2R_m - L)}. \tag{18}$$

Specifically, for a 5 cm CFP, the Rayleigh range, z_0, is:

$$z_0 = \frac{1}{2}\sqrt{5(2 * 5 - 5)}$$

$$z_0 = 2.5cm \tag{19}$$

The beam waist is defined in terms of the Rayleigh range and the wavelength, λ :

$$w_0 = \sqrt{\frac{\lambda z_0}{\pi}}. \tag{20}$$

For the specific case with light at 633 nm and the z_0 of 2.5 cm calculated above, the value for w_0 is 71 μm. The waist represents the $1/e^2$ half-width of the beam at the center of the CFP, making the $1/e^2$ full-width 142 μm. To determine the waist of a 62.5 μm core fiber the V parameter is calculated. The V parameter is used to characterize the number of modes coming out of a fiber. Mathematically, the V parameter is expressed as [18]:

$$V = 2\pi \frac{a}{\lambda_0} NA, \tag{21}$$

where a is the radius of the fiber, λ_0 is the wavelength of the laser, and NA is the numerical aperture of the fiber. The numerical aperture is defined as:

$$NA = nsin\theta, \tag{22}$$

where n is the index of refraction and θ is the half angle of the light emitted from the fiber. The NA for a particular fiber is known, and the angle with which light is emitted from the fiber is solved for. The V parameter for the CFP being used is:

$$V = 2\pi \frac{31.25x10^{-6}}{633x10^{-9}} 0.22, \tag{23}$$

such that V=68. In a publication by G. Agrawal [18], a plot of the V parameter vs. w/a is shown, where w is the $1/e^2$ beam half-width and a is the radius of the fiber core. The waist of the fiber can best be estimated for a V parameter between one and three, which is substantially smaller than the 68 calculated for the 62.5 μm fiber. While the plot of the V parameter vs. w/a appears to approach an asymptote for a V of 7 and beyond, the value for a V of 68 is not well established. Assuming the asymptotic behavior continues to large values of V, the corresponding, w/a is approximately 0.7. The value for a is known to be 31.25 μm. The beam $1/e^2$ half-width is then 22 μm,

or 44 μm for the $1/e^2$ full-width. The ratio of the Gaussian beam waist to the fiber waist determines the magnification factor, M:

$$\frac{f_2}{f_1} = M = \frac{142\mu m}{44\mu m} = 3.2. \tag{24}$$

To achieve the mode-matched condition, the focal length of the first lens must be roughly three times the focal length of the second lens, to maintain the appropriate magnification factor, M. For a 62.5 μm fiber, a magnification factor of three yields a waist size of 188 μm, using the imaging equation to determine the waist. Mode-matching multimode beams is not achievable, as higher-order modes do not collapse into one focus. The focus of the multimode beam produces a much broader focus at the center of the CFP. To truly mode-match a CFP, a single mode beam must be used, such that a Gaussian approximation is valid. By eliminating modes into the CFP the mode-matched condition is approached as the number of modes is reduced and the CFP tends towards a single mode solution. The reduction of the number of modes into the CFP is demonstrated in the Experiment section and the magnification factor found here is used to determine the effectiveness of nominally mode-matching into the CFP.

Multimode Beams

Multimode beams are used in the experiment to simulate the conditions of the intended use of the CFP, which is to capture light that has been scattered by the atmosphere. A Gaussian beam approximation is not valid for multiple spatial modes, instead a Hermite-Gaussian solution is necessary. A Hermite-Gaussian distribution represents the higher-order spatial modes which are present when using multimode fibers. A mode within a CFP can be thought of as a field distribution within the CFP,

which once established by passing through the CFP once, remains unchanged and is only multiplied by a constant amplitude factor [1]. The Hermite-Gaussian distribution represents a family of solutions that have different amplitude distributions [19]. If the cavity is mode-matched to a Gaussian beam, the Hermite-Gaussian modes will fit into the CFP as well, as the solution is an extension of the Gaussian solution.

The Gaussian beam approximation yields only the most basic of information for a multimode beam propagating through a CFP, ensuring only that the family of Hermite-Gaussian higher-order modes will be a solution for the CFP. Experimentally, however, a multimode beam will not resemble characteristics and behaviors of a Gaussian beam, as there are far too many interactions of the higher-order modes within the CFP to predict from a first-order approximation. The approach in applying Gaussian beam characteristics to a multimode beam is to understand the behavior from a Gaussian perspective and proceed knowing that the experiment will differ from the predicted. If Gaussian beam characteristics are present, they can be differentiated from the other behaviors that can then be attributed to higher-order modes.

The following argument closely follows Hercher's outline of mode considerations in a CFP [3]. If a multimode beam that is incident upon a CFP can be decomposed into many transverse modes, TEM_{qmn}, then the resonance will occur for a mirror separation, d, of:

$$d = \frac{\lambda}{2}[q + \frac{1}{\pi}(1 + m + n)cos^{-1}[(1 - \frac{L}{\rho_1})(1 - \frac{L}{\rho_2})]^{1/2}], \tag{25}$$

where λ is the wavelength of the incoming light, m and n represent eigenmodes, and q represents the number of axial modes that fit within the cavity. The L is the length of the cavity, and the values of ρ represent the radii of the two mirrors. If the configuration is confocal, equation 25 significantly simplifies to:

$$d = \frac{\lambda}{4}[2q + (1 + m + n)]. \tag{26}$$

The significance of equation 26 is that there are no longer phase considerations and all of the transverse modes will resonate at a specific length of the CFP. If there are an equal number of odd and even modes, then the values for q, m, and n can be lumped into a quantity, l, such that l is an integer, and the length of the CFP is:

$$d = \frac{\lambda l}{4}. \tag{27}$$

Equation 27 demonstrates that all of the transverse modes are degenerate, for an integer number of quarter wavelengths, thus the CFP will automatically be mode-matched for all spatial modes. The beams considered throughout Hercher's paper [3] were coming into the CFP collimated. In many circumstances, including those considered herein, the beam does not come into the CFP collimated. An argument was made by Munnerlyn and Balliett [4], which stated that although theoretically a CFP does not need to be mode-matched to attain a high finesse or high transmission through the CFP, it does aid when the beam sent into the CFP is not collimated [4]. It is argued and demonstrated that mode-matching into the CFP is highly advantageous and increases the transmission through the CFP by a factor of two [4].

An understanding of the basic construction of a CFP and the way light travels through the CFP was addressed. Important parameters for characterizing the CFP such as finesse, FSR, reflection, and transmission through the cavity, as well as mode-matching using a Gaussian approximation are discussed. All theoretical considerations will aid in the experimental analysis of the CFP, understanding the caveat of the experimental CFP operating with many higher-order modes, rather than as a Gaussian beam.

MODELING

One of the advantages of the CFP cavity is the characteristic of maintaining an optical resonance for multiple spatial modes. Light must be mode-matched into the CFP carefully to maintain the optical resonance. In this chapter, a ray tracing model used to explore mode-matching light into a CFP is described. Also, parameter spaces that are to be experimentally probed are modeled here to determine the potential boundaries. Results from this model for a CFP using both spherical and parabolic mirrors are presented, as well as CFP models with high finesse.

Outline of Model

The ray-tracing model used to study the effects of mode-matching on the CFP was developed using the Matlab programming environment. The model can be found in Appendix A. The model begins ray tracing at the center of the CFP, as depicted in Figure 8. The distances are calculated for each of the five segments that form one complete roundtrip within the CFP. Inputs to the model include the slope and the wavelength of the incoming light, the beam size, the radius of curvature of the mirrors and the shape of the mirrors. An array of slopes is entered into the model to determine, as a function of angle, how the optical path length differs through the CFP. The finesse for the CFP can be estimated with the ray tracing model by realizing that the finesse is proportional to the number of passes a ray makes within the CFP. For example, if there are 200 roundtrips through the CFP, then the finesse is 200. The y_0 parameter determines the offset of the beam from the optical axis. It is meant to represent the beam size radius from a multimode fiber; however, only a single ray is sent from the offset point, which does not simulate a real multimode

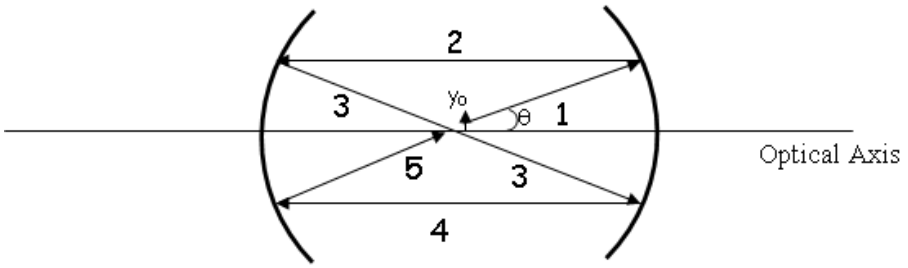

Figure 8: The CFP and the order in which Matlab calculates each segment is shown. The y_0 is the beam radius and θ is the angle with which the light enters into the CFP. Both y_0 and θ are measured from the optical axis.

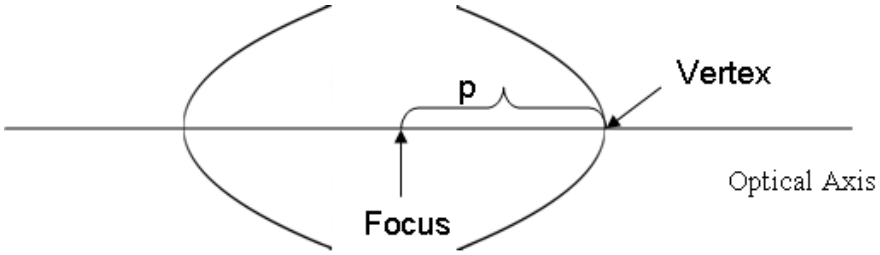

Figure 9: A confocal parabola with the parameter p defined as the distance between the vertex and the focus of the parabola.

beam. This must be taken into consideration when assessing the accuracy of this model to predict experimental results.

For a parabolic mirror, the parameter p is considered, where p is the distance from the vertex to the focus of the parabola depicted in Figure 9. For a parabola with a radius of curvature of 5.0 mm, the value of p is 2.5 mm, or half of the radius of curvature.

Model Results

Spherical vs. Parabolic Mirrors

Both spherical and parabolic mirrors were considered. One roundtrip pass through the CFP was analyzed for each conic mirror. In Figure 10, the region of interest is

marked with two lines at ±6.33 nm, which is one hundredth of the laser wavelength at 633 nm and corresponds to a phase shift of $2\pi/100$ or 63 milliradians (mrad). This region represents the amount that the light can be out of phase and still constructively interfere. Figure 10 shows the deviation from a perfect pass through a 5 cm cavity and is plotted as a function of the angle of incoming light into the CFP. The optimal path length for a 5 cm CFP is 4L, or 20 cm, where L is the length of the cavity. An optical path length difference of 0 corresponds to a 20 cm path length. The solid lines in the figure represent 6.33 nm deviations from a perfect pass through the CFP. Several different beam radii were input to the model by offsetting the input on the y-axis, represented by y_0 in Figure 8.

In Figure 10, it is shown that fibers with a beam radius of 100 μm and smaller have accepted angles from 0 mrad to 59.55 mrad. Waists larger than 100 μm in radius have acceptable phase difference for specific angular regions. A 200 μm waist has acceptable phase from 75 to 85 mrad. For larger waists, the area where their curves intersect the region of interest are minimal.

For the parabolic mirror cavity, 20 μm fibers and below accept all incoming angles. A 20 μm fiber is slightly larger than a single mode fiber. For multimode fibers, the acceptance angle extends from 0 mrad to a maximum of 40.1 mrad. The spherical mirrors perform as well or better than the parabolic mirrors for multimode beams. Since spherical mirrors perform well and are more readily available than other conics, they are used for the experiment and the rest of the modeling.

High Finesse Models

Various finesses were modeled by increasing the number of roundtrip passes from 1 to 100, 200, 300, and 400. A single mode fiber, 100 μm, and 200 μm core fiber were modeled. It is assumed that the fiber diameter size and the waist size in the center of

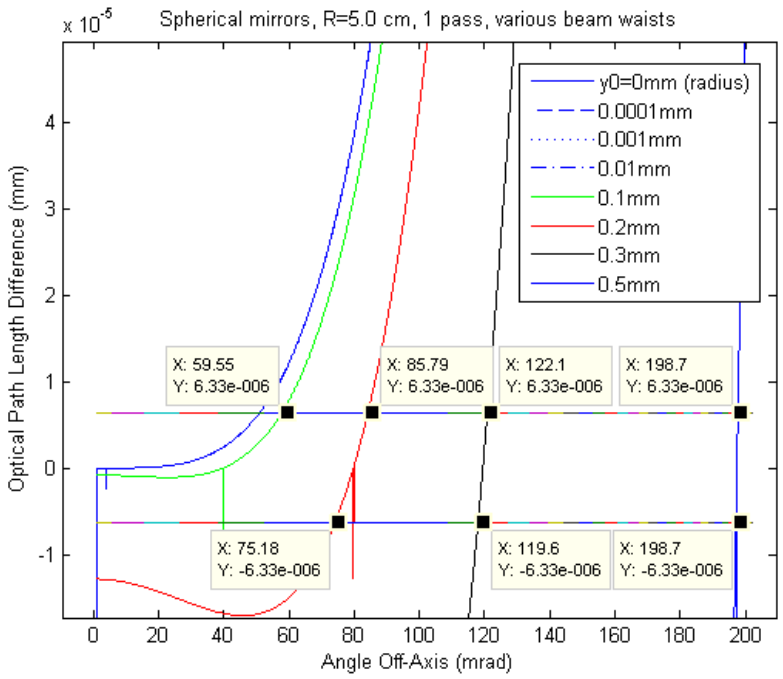

Figure 10: The model results for spherical mirrors, with a finesse of one, and several beam waists considered.

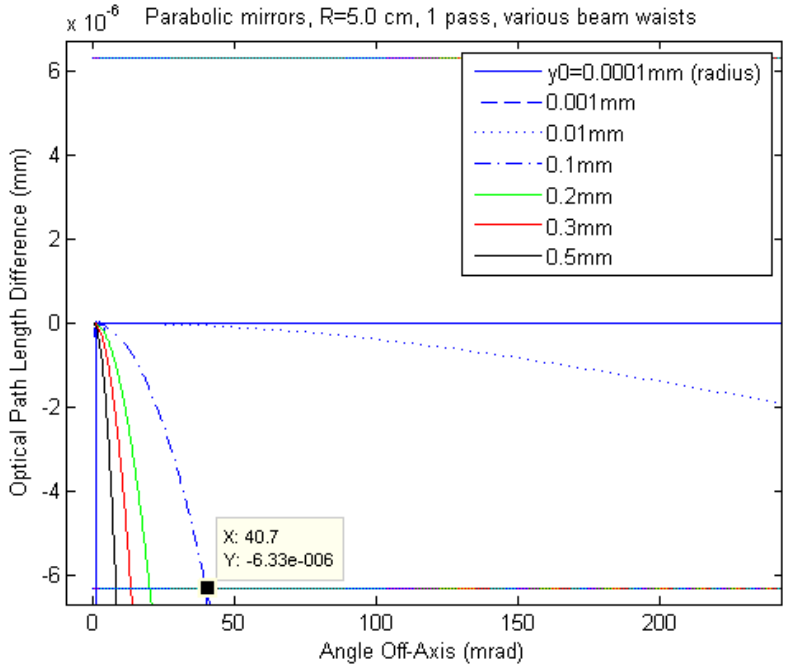

Figure 11: The model results for parabolic mirrors, with a finesse of one, and several beam waists considered.

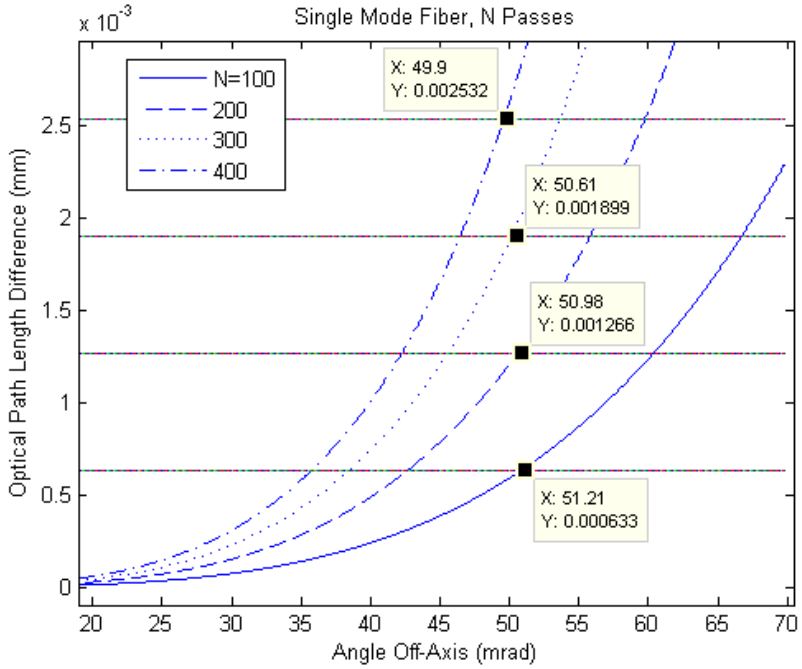

Figure 12: The optical path length difference as a function of angle for a single mode fiber where input finesses vary from 100 to 400. The tolerance of optical path length difference is different for each finesse, the intersection for each finesse is marked.

the CFP are the same; therefore the magnification factor of the fiber to the CFP is one. The results are depicted in Figures 12 through 14. As the finesse increases, the tolerance of the phase increases by the original phase difference multiplied by N, the number of passes through the CFP. As the number of passes, or finesse, increases, the range of accepted angles decreases. The decrease with finesse is due to walk-off, which is the increase in the beam diameter due to the multiple reflections. This decrease in the acceptance angle is more prevalent in the 100 μm and 200 μm core fibers, although the range of accepted angles is larger for these fibers than the single mode fiber, as shown in Figures 12 through 14. The range of accepted angles into the CFP does not vary greatly with the finesse. From the model, experimental performance can be estimated. The product of the beam waist size at the center of the CFP and the incoming angle to the CFP is determined for each finesse and each fiber, seen in

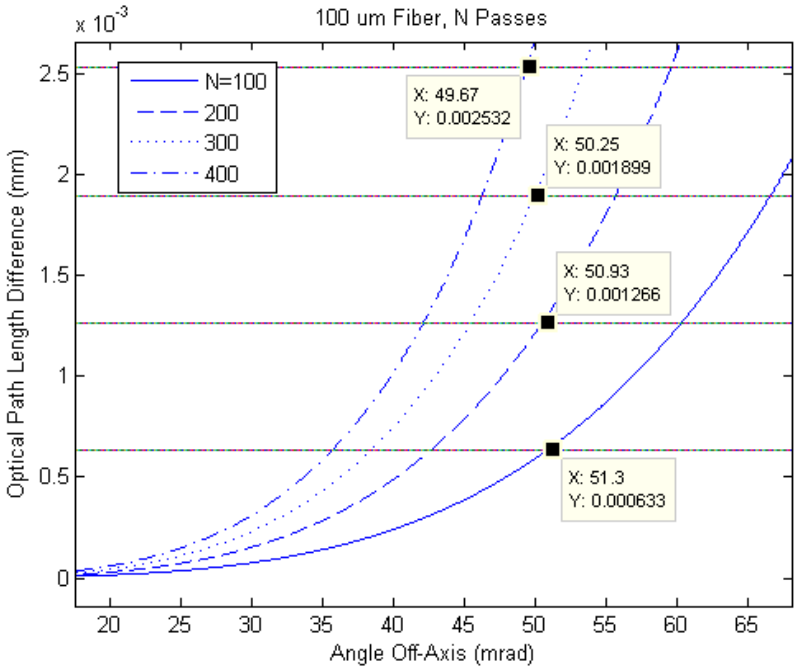

Figure 13: The optical path length difference as a function of angle for a 100 μm core fiber where input finesses vary from 100 to 400.

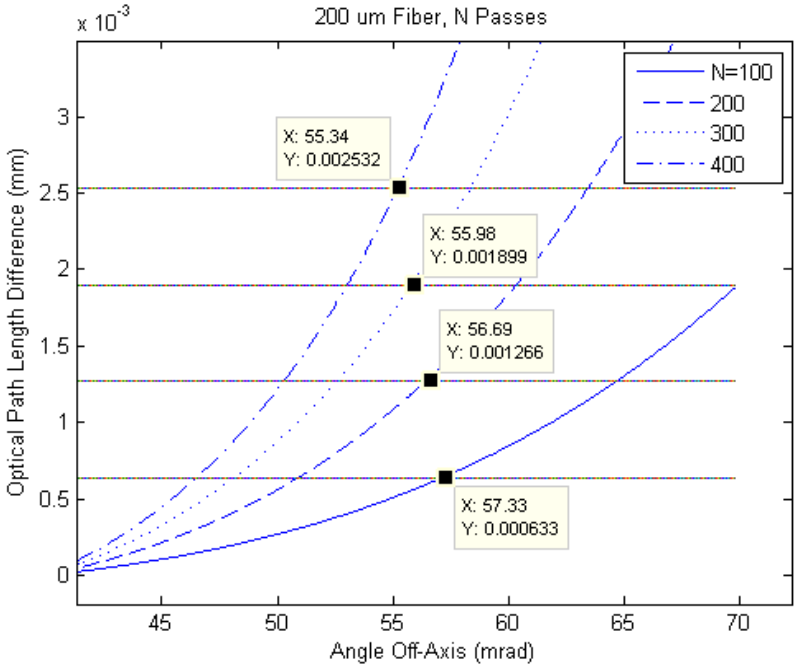

Figure 14: The optical path length difference as a function of angle for a 200 μm core fiber where input finesses vary from 100 to 400.

Table 1: The waist-angle product is depicted for each fiber and each finesse. The diameter of the single mode fiber was taken to be 8 μm. The range is the range of angles accepted in Figures 12 through 14 above, converted from degrees to milliradians. The angle represented is the full-angle, and the waist represented is the diameter.

Finesse	Single Mode		100 μm		200μm	
	Range (mrad)	Product (mm mrad)	Range (mrad)	Product (mm mrad)	Range (mrad)	Product (mm rad)
100	102.2	0.82	103.6	10.4	114.6	22.9
200	101.8	0.81	102.4	10.2	113.0	22.6
300	100.4	0.80	100.6	10.1	111.8	22.4
400	98.8	0.79	98.8	9.88	110.8	22.2

Table 1. Experimentally, it should be possible to achieve these results with the same conditions entered into the model.

Model Verification

The model of the CFP takes into account the spherical nature of the mirrors. The optical path length difference calculated for each offset from the optical axis should correspond with the optical path length difference calculated for spherical aberration effects. With light coming in to the CFP on-axis the model traces out the optical path through the cavity and the only deviation from a perfect pass through the cavity of 4L, where L is the length of the cavity, should be due to the spherical nature of the mirrors. A comparison of the optical path length difference due to the spherical aberration shown in equation 3 and the optical path length difference found by the model is shown in Figure 15. The angle considered is zero, as the analysis takes place for collimated light. There is no difference between the path lengths predicted by the model and the theoretical spherical aberration, demonstrating that the model successfully follows theoretical considerations for light coming in to the

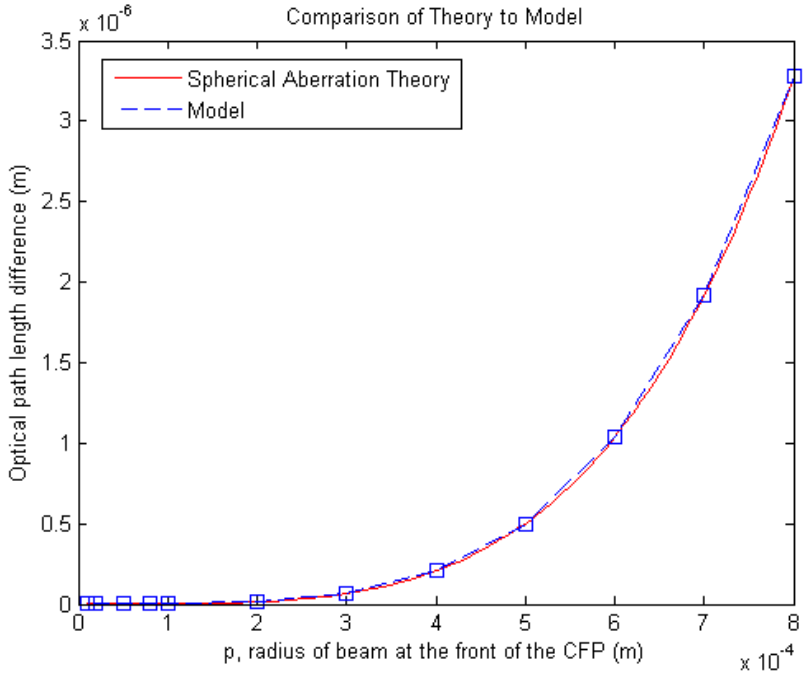

Figure 15: A comparison between the results of the optical path length calculated in the model and the optical path length difference due to the effect of spherical aberration.

CFP collimated. There are other aberrations to consider for off-axis light coming into the CFP that are not accounted for in the model.

The model demonstrates that a parabolic CFP is no more advantageous than a spherical CFP in terms of the desired parameters; thus spherical mirrors are used. According to the model, the CFP can support high finesses, up to 400, and fiber diameters up to 200 μm. The accepted incoming angle for these parameters is 52.4 mrad, the full angle being 104.7 mrad. An important caveat is that to simulate multimode beams, only one beam is being put into the cavity, off-set from the axis by the diameter of the fiber. Also, the model starts with the source in the center. These two variations from the actual experiment may have an effect on the experimental results.

EXPERIMENT

Designing the Confocal Fabry-Perot Cavity

A CFP cavity was designed and built. The schematic of the cavity is shown in Figure 16. The general design consists of a cylindrical ceramic piezo-electric tube (PZT) between two mirrors. One of the mirrors is fixed, while the other one is adjustable. The distance between the two mirrors needed to achieve the confocal configuration is 5 cm, leading to a FSR of 1.5 GHz.

The PZT is 2.54 cm long and 2.54 cm in diameter. The wall thickness of the PZT is 0.31 cm. The material composition of the PZT is lead zirconate titanate [17]. A voltage applied between the inner and outer walls of the PZT causes the length between the two mirrors to change. Two delrin rings hold the PZT on both sides, as delrin is not conductive. The delrin pieces are displayed in black in Figure 16. The remainder of the cavity is made of aluminum, with the exception of one brass piece, as seen in Figure 17. The mirror shown at the right of the CFP is fixed in place. The mirror shown at the left of the CFP is held in a brass ring that can slide in the aluminum housing. This allows adjustment of the coarse CFP length such that the confocal configuration can be achieved. The brass ring is locked in place using six set screws. Both mirrors sit on o-rings, shown in Figure 16, which allow them to sit evenly in the metal pieces without undue stress on the mirror substrates. The final aluminum piece, attached to the brass piece with the mirror, can be attached to a Newport Universal Motion Controller/Driver, which can make fine adjustments in 50 nm increments, necessary to finding the exact confocal location. The whole CFP is held together with $\frac{1}{4}$ - 20, 2 inch long set bolts that run through the whole CFP. The

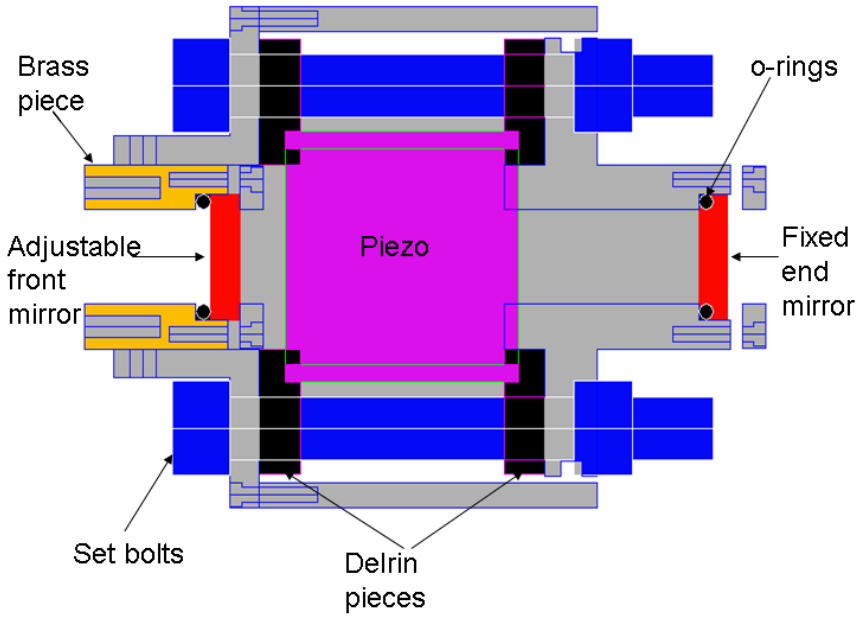

Figure 16: The schematic of the CFP cavity design.

mirrors are 12.7 mm in diameter. They both have a radius of curvature of 5 cm and are coated for the spectral region of 525 nm to 650 nm.

Alignment

The following is the procedure used for aligning the CFP in its confocal configuration. Light from a frequency stabilized helium-neon (HeNe) laser was launched into a multimode optical fiber. The output from the fiber was collimated using a lens with a focal length of 300 mm. Light is then directed to a focusing lens with a focal length of 750 mm. After the focusing lens, two steering mirrors provide the necessary adjustment to direct the light into the CFP. The CFP is placed such that the center of the CFP is located at the focus of the focusing lens. Light passing through the CFP is focused onto a New Focus 2001 photodetector. The photodetector is monitored using an oscilloscope.

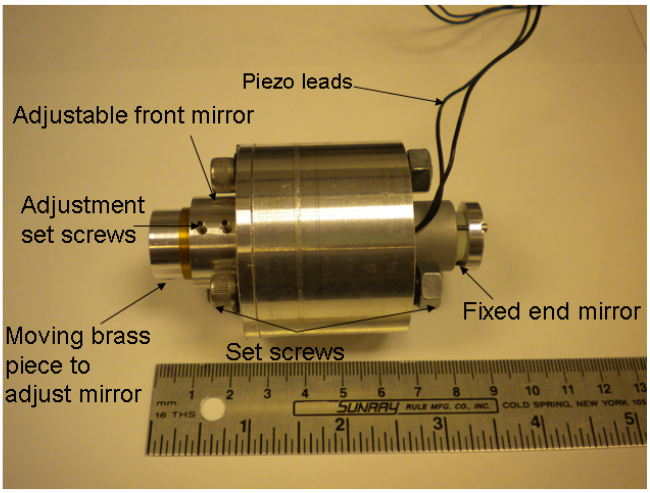

Figure 17: The machined CFP cavity.

Scanning the CFP is achieved by supplying a high voltage signal to the PZT within the CFP. A commercial Burleigh Programmable Ramp Generator RC-44 driver was used to provide the high voltage required to scan through at least one FSR of the CFP.

The coarse mirror spacing is adjusted and the CFP transmission is monitored. The confocal condition is achieved when the output of a CFP is a perfectly symmetric peak, with the slopes on each side being equal, shown in Figure 19c. If the coarse mirror spacing is long, then the peak will splay out to the right, as seen in Figure 19a. If the mirror spacing is too short, the peak splays to the left as seen in Figure 19b.

To find the optimal confocal condition of the CFP, the six set screws on the adjustable mirror side are loosened. The screws can then be tightened such that the brass piece only slightly slides back and forth. Adjustment of the coarse mirror spacing is achieved either by hand or with a Newport Universal Motion Controller/Driver.

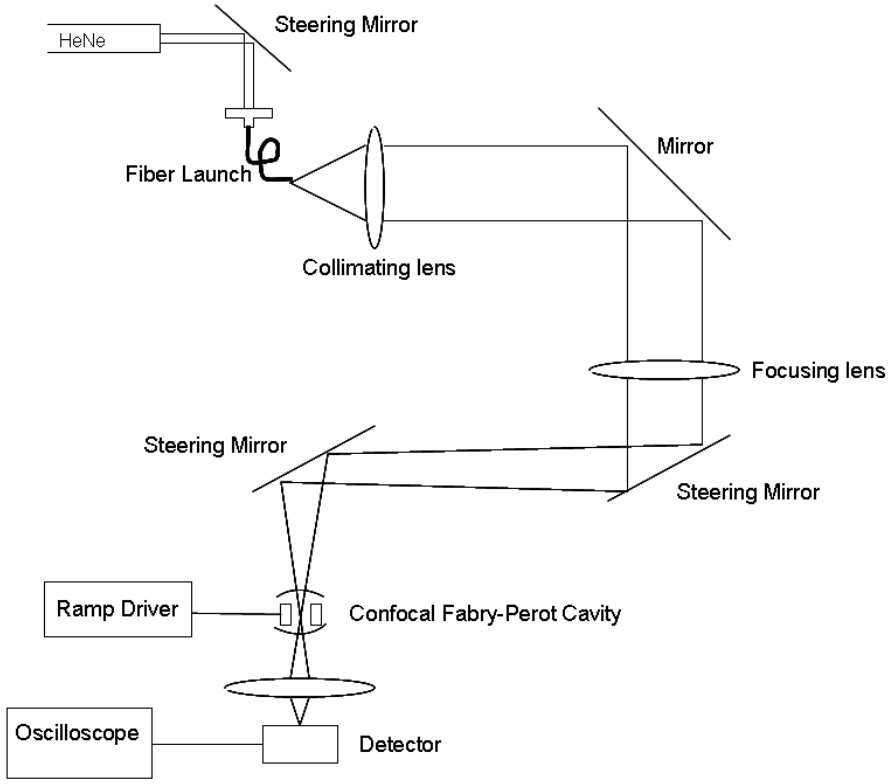

Figure 18: An example of an alignment setup for the CFP cavity.

The automated driver allows for finer adjustment, with a computer controlled resolution of 50 nm.

Two Lens Experiment

The CFP was characterized experimentally in two ways. The purpose of the two experiments was to determine the behavior of the CFP by varying different parameters and finding certain trends associated with the CFP. The parameters explored were those likely to change when the CFP is to be utilized in a larger optical system or instrument. The two parameters of main interest were the angle of the light incoming to the CFP and the size of the waist at the center of the CFP. The characteristics monitored were the finesse, reflection, and transmission of the CFP.

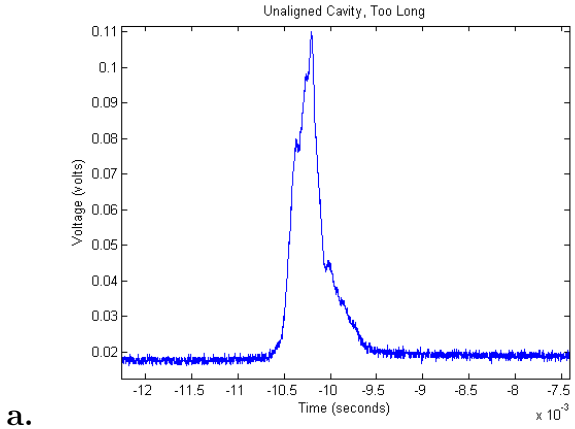

a.

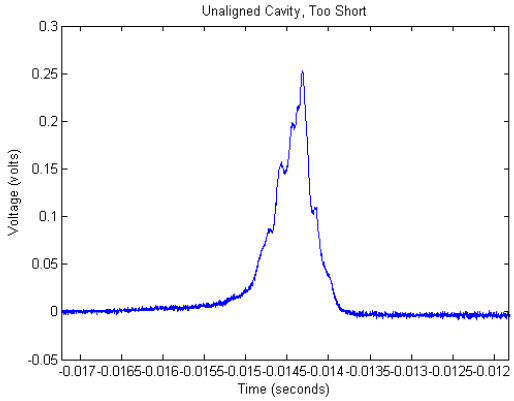

b.

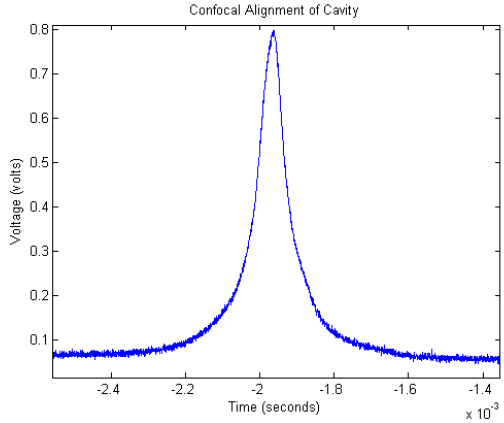

c.

Figure 19: a. Depicts a CFP in which the mirrors are spaced too far apart, b. represents a CFP with mirrors that are spaced too close together, and c. shows a well aligned CFP.

The two experiments were a two lens experiment and a one lens experiment. In the two lens experiment, the waist was changed by varying the magnification factor of the two lenses' focal lengths. The angle was changed by adjusting the aperture of an iris, which also limited the number of modes in the CFP. The single lens experiment was conducted such that the waist and the angle were varied simultaneously by adjusting the distance of the CFP with respect to the lens and the lens with respect to the fiber.

The setup of the two lens experiment is shown in Figure 20. The two lens setup measures the light reflected off of the CFP, the light transmitted through the CFP, the light incident on the CFP, and the finesse of the CFP. The light is launched from a frequency stabilized HeNe into a fiber. The output of the fiber is collimated with a lens, which is placed nominally a focal length away from the fiber. The collimated light is sent through an iris, which is placed immediately before the focusing lens. After the focusing lens, there is a flipper mirror, which, when up, sends light into the incident detector to measure how much light is incident upon the CFP. If the flipper mirror is down, the light goes through a polarizer. The light is next incident on a quarter wave plate, which creates circularly polarized light. The light is then directed to two steering mirrors, which guide the light into the CFP. The light coming out of the CFP is focused onto a detector measuring the transmission. The light reflected from the cavity passes back through the quarter wave plate, creating linearly polarized light that is rejected by the polarizing cube. This rejected light is monitored using a third detector. The detectors are calibrated with each other and the losses through each optic are known. This allows for the measurement of the percentage of the incident light that is transmitted through the cavity and the percentage of the light that is reflected from the cavity.

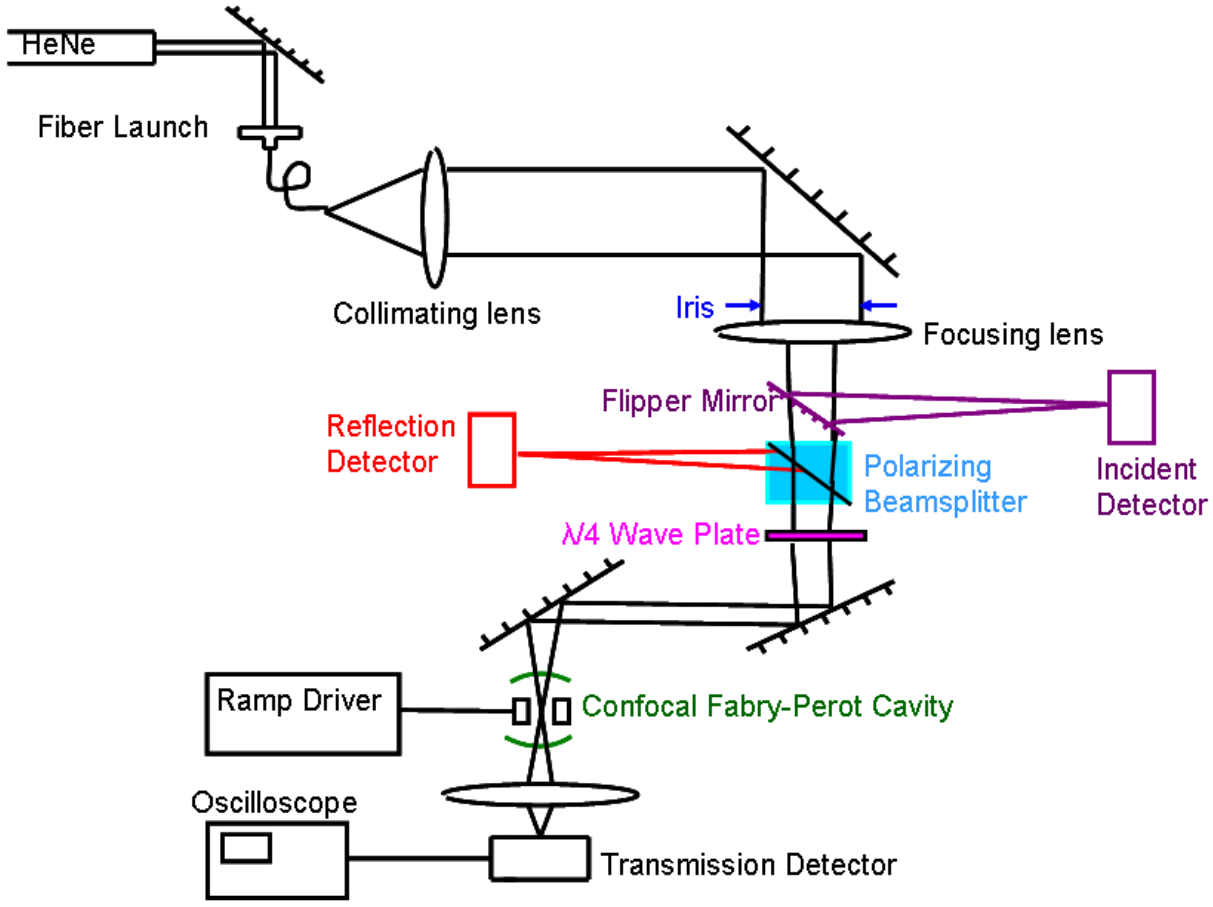

Figure 20: The schematic of the two lens experiment setup.

The parameter space being explored with the two lens experiment is the incoming angle to the CFP and the size of the waist at the center of the CFP. To vary the incoming angle to the CFP, which does not alter the waist, the iris preceding the focusing lens is adjusted. The one caveat to this method of altering the angle is that by decreasing the iris aperture, modes are excluded from entering the CFP. The effect on the number of modes is considered in the analysis of this experiment. By reducing the number of modes into the cavity, the mode-matched condition will be approached, as the cavity tends towards a single mode. To change the waist size at the center of the CFP, different lenses are used for the collimating and focusing lenses. The ratio of their focal lengths yields different beam waists at the center of the CFP. Since large multimode fibers are being used, the image equation is used to determine the spot size in the center of the CFP:

$$w = d_f \frac{f_2}{f_1}, \tag{28}$$

where d_f is the diameter of the fiber, and f_2 and f_1 are the focal lengths of the focusing and collimating lenses respectively. The mode-matching condition for a single mode fiber was determined in equation 24. The ratio of the focal lengths, f_2/f_1, was roughly three. For this experiment 750 mm and 250 mm focal length lenses were used to achieve a magnification of three, as seen in Table 2. For other fiber diameter sizes to achieve a waist of 190 μm the configurations are italicized in Table 2. As each of these fibers approaches fewer modes, the mode-match condition is approached.

Results of Two Lens Experiment, 5 cm CFP

The results for the finesse, reflection, and transmission are shown in Figures 21 to 25. The finesse results are plotted with the angle on the y-axis, the waist size on the x-axis and the finesse in color on the z-axis. All of the finesse plots are scaled the same, with the finesse ranging from 60 to 350. The reflection and transmission

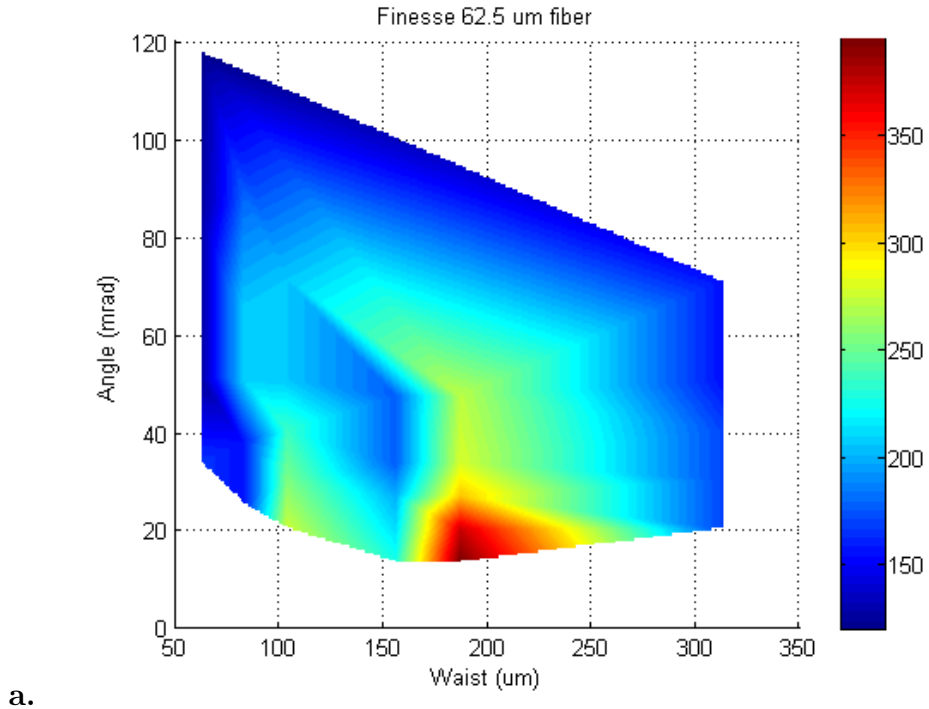

a.

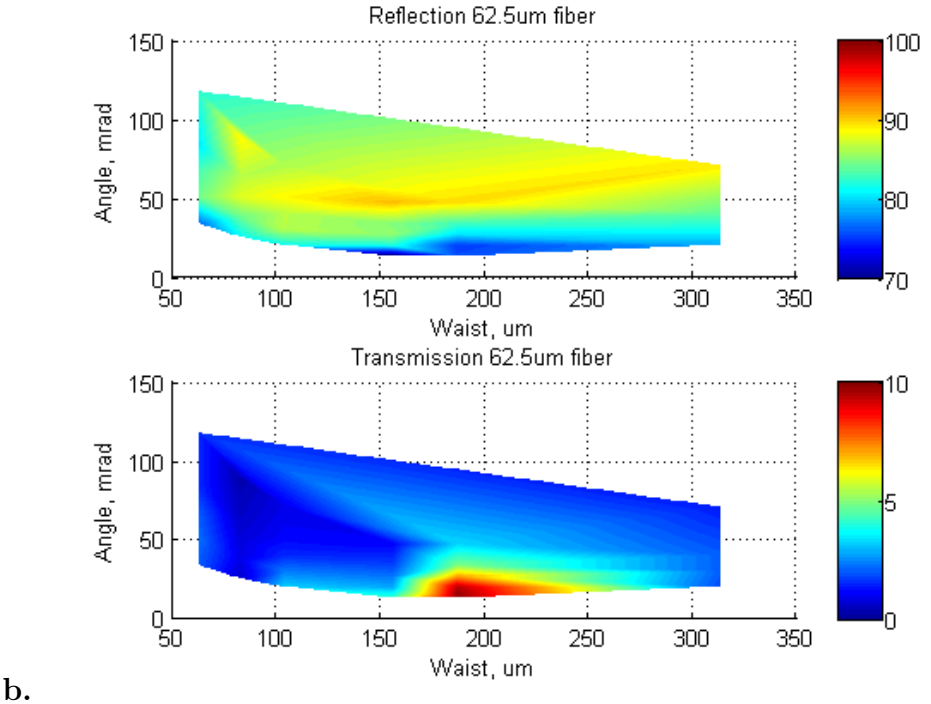

b.

Figure 21: a. The finesse as a function of angle and beam waist for a 62.5 μm fiber, b. The corresponding reflection and transmission of the CFP also as a function of angle and beam waist for the 62.5 μm fiber.

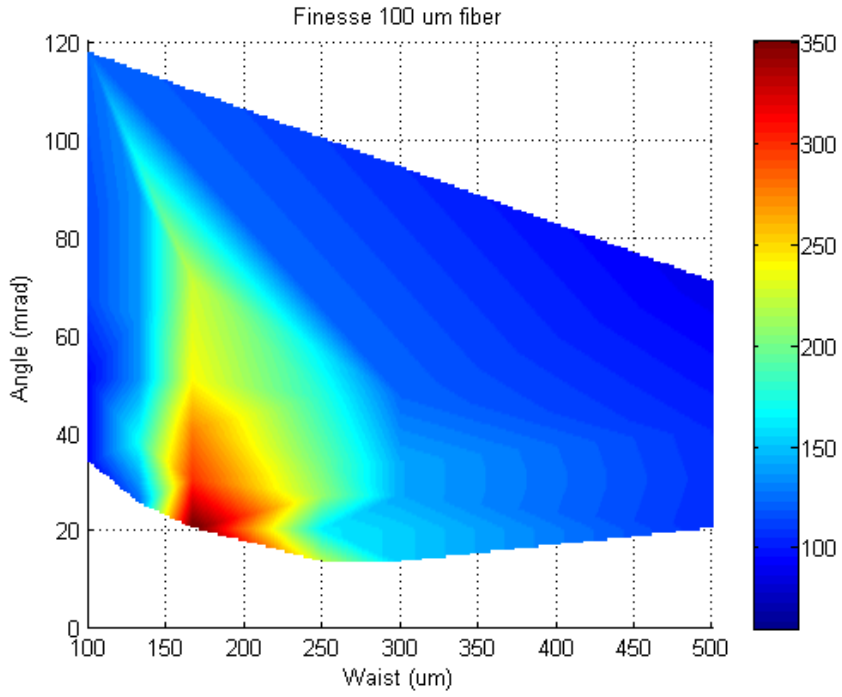

a.

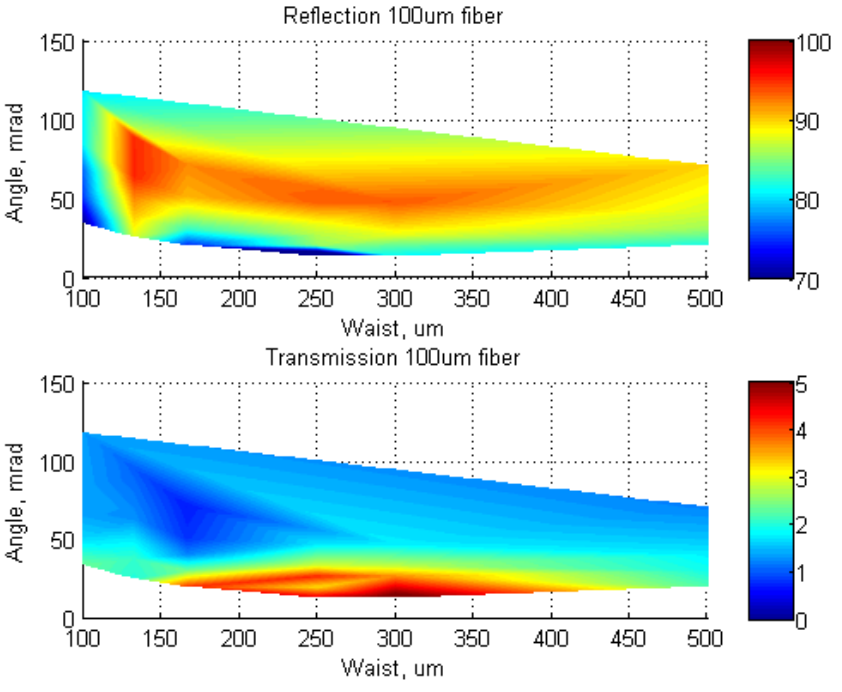

b.

Figure 22: a. The finesse as a function of angle and beam waist for a 100 μm fiber, b. The corresponding reflection and transmission of the CFP also as a function of angle and beam waist for the 100 μm fiber.

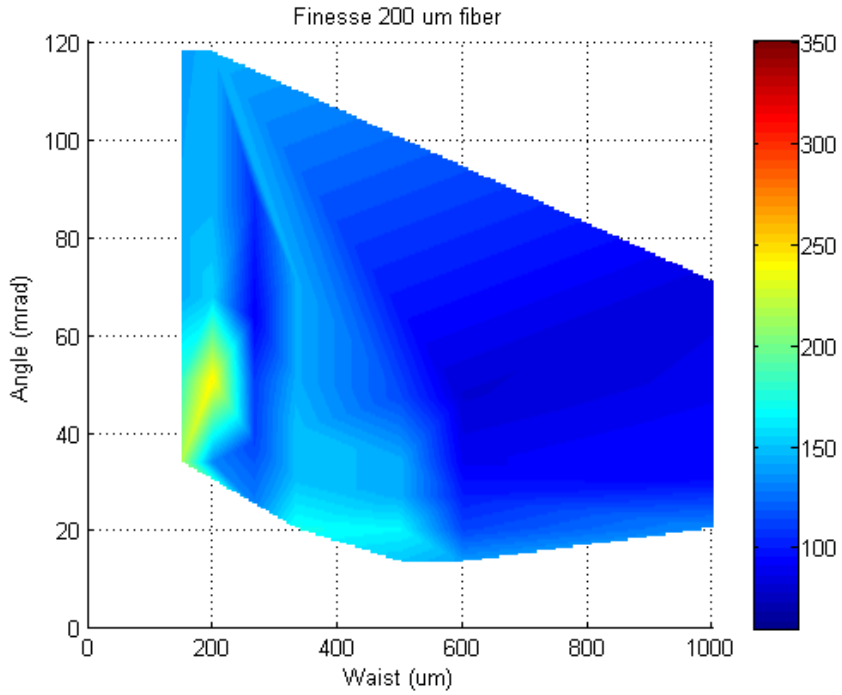

a.

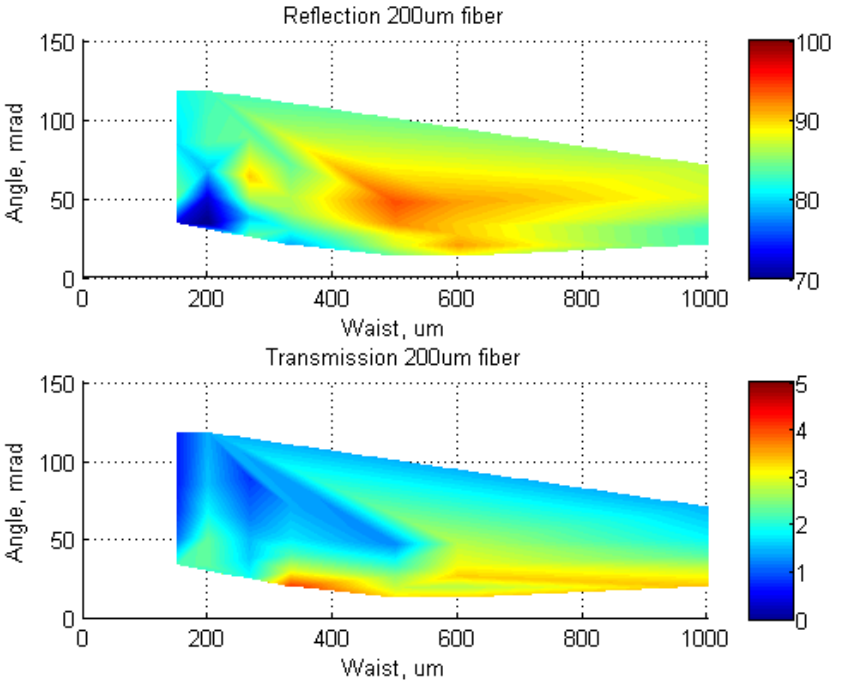

b.

Figure 23: a. The finesse as a function of angle and beam waist for a 200 μm fiber, b. The corresponding reflection and transmission of the CFP also as a function of angle and beam waist for the 200 μm fiber.

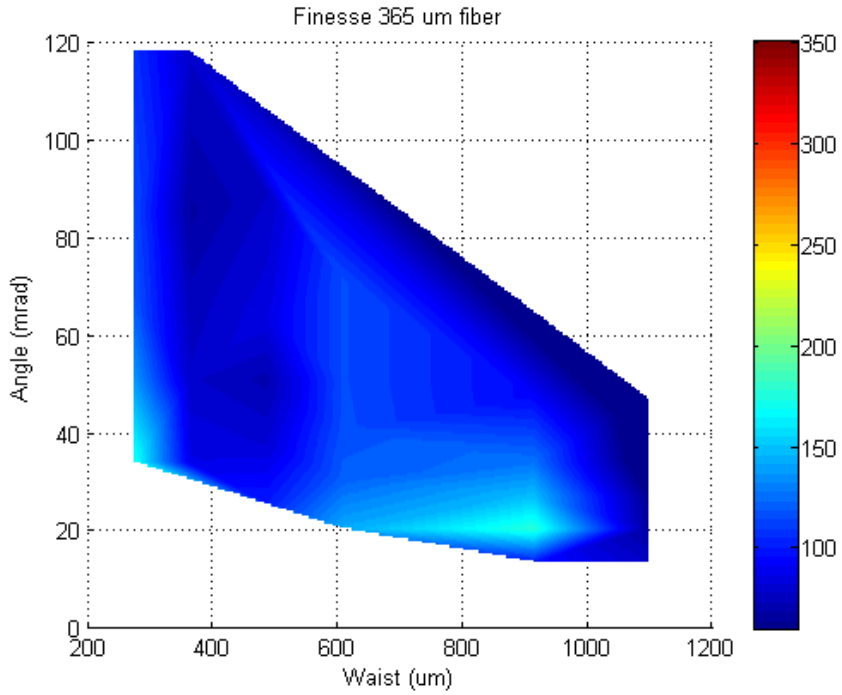

a.

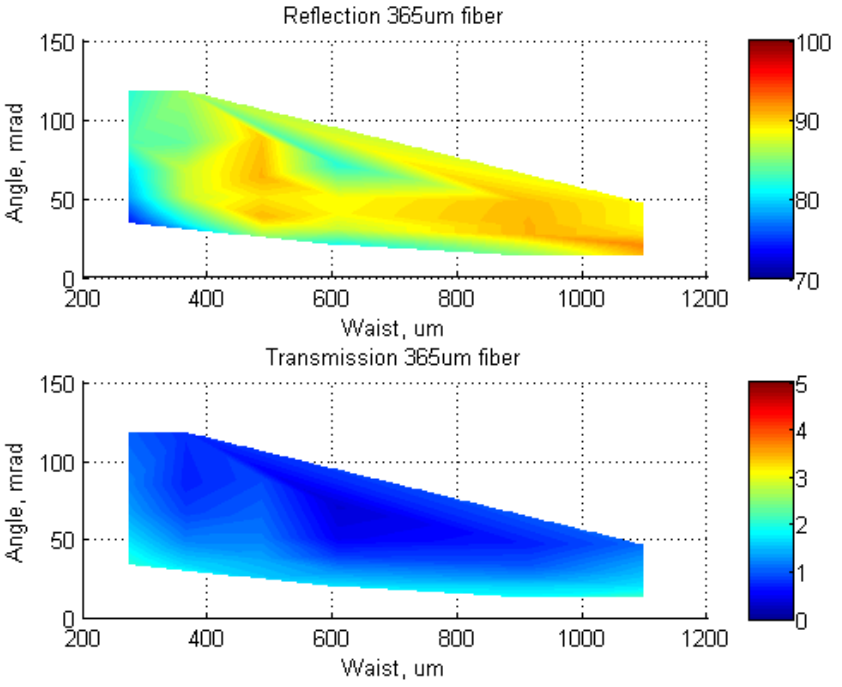

b.

Figure 24: a. The finesse as a function of angle and beam waist for a 365 μm fiber, b. The corresponding reflection and transmission of the CFP also as a function of angle and beam waist for the 365 μm fiber.

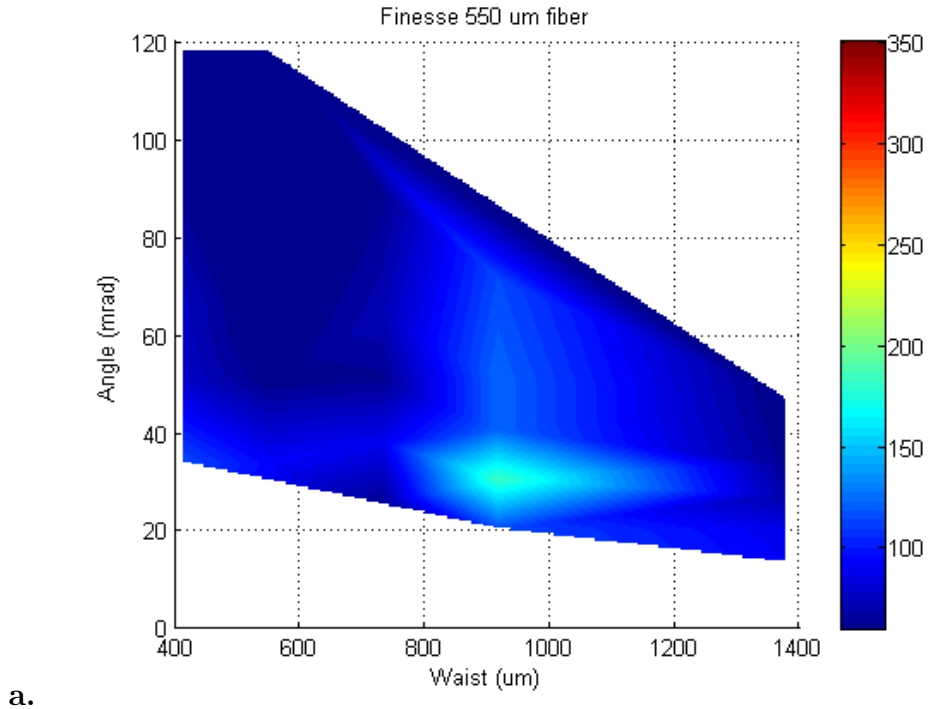

a.

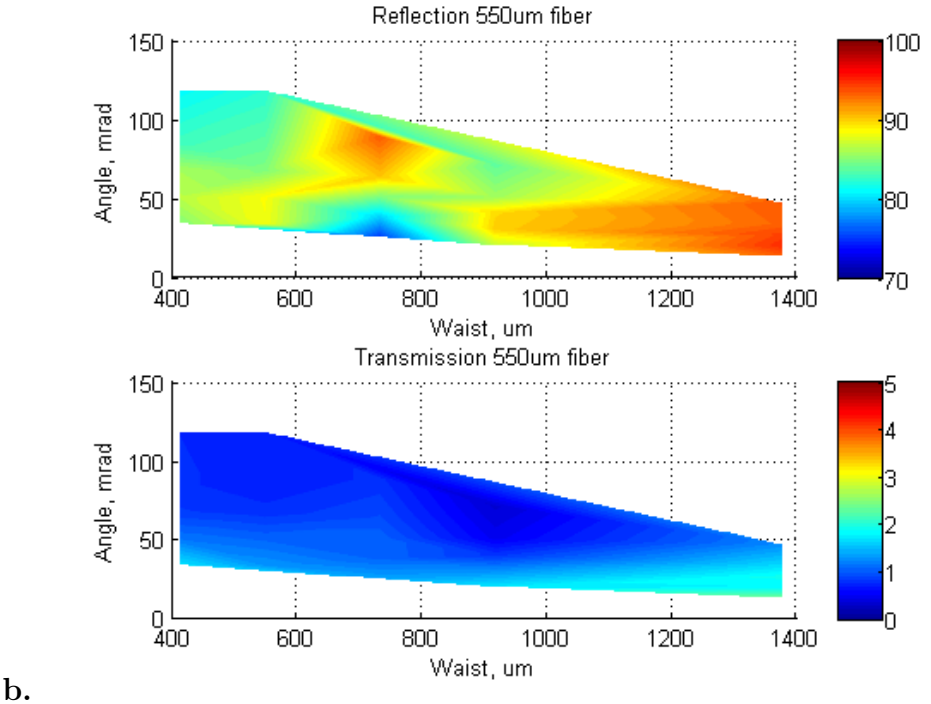

b.

Figure 25: a. The finesse as a function of angle and beam waist for a 550 μm fiber, b. The corresponding reflection and transmission of the CFP also as a function of angle and beam waist for the 550 μm fiber.

Table 2: The data taken to find the reflection, transmission, and finesse of the CFP is shown. The left column shows the diameter of the multimode fibers. The top row shows the lens pair combinations used to vary the beam waist. To find if a data set was taken for a particular fiber and lens combination, find the lens combination, say 500/100 and a 200 μm fiber. Where the column and row meet indicates the waist size at the center of the CFP, for this example, the waist size is 1000 μm or 1 mm. Nominally mode-matched waist sizes are italicized.

Fiber (um)	Lens configurations to determine beam waist, f_2/f_1 (mm)						
	500/100	750/250	750/300	500/300	400/300	300/300	300/400
62.5	310 um	*187.5*	156.25	104	83.3	62.5	
100	500	300	250	*166.7*	133.3	100	
200	1000	600	500	333.3	266.7	*200*	150
365		1095	912.5	608.3	486.7	365	273.75
550			1375	916.7	733.3	550	412.5

plots are plotted with the same x and y-axes as the finesse plots. The reflection and transmission are on the z-axes. The scale for the reflection is 70% to 100% of light being reflected from the CFP. The scale for the transmission is 0% to 5%, except in the case of the 62.5 μm fiber, where the transmission extends from 0% to 10%. For each fiber, between five and seven data sets were gathered, as seen in Table 2. The data was input to Matlab, which performed an interpolation between each data point to result in the contour plots presented here.

For the 62.5 μm fiber, there were six sets of data gathered. The finesse is largest at an angle of 13.5 mrad and at a waist of 187 μm. The finesse at this angle and waist was measured to be 393. Transmission through the CFP at the same waist of 187 μm, was 9.8%, the highest transmission through the CFP of any configuration. The reason for high transmission and finesse at the waist of 187 μm is because the CFP is mode-matched at this waist. The angle is small because the iris is stopped down to a small aperture, such that most of the modes of the multimode fiber are blocked

from the CFP. The multimode nature of the beam is tending towards a single mode fiber, which is theoretically what the CFP is mode-matched to, yielding high finesse.

Similarly, the 100 μm fiber behaves with the same tendencies as the 62.5 μm fiber. There is a high finesse region, reaching a peak finesse of 358, at an angle of 20.3 mrad and at a waist of 167 μm. The transmission reaches 4.5% at small angles, while conversely, the reflection is low at low angles, but increases with larger angles and waists.

The highest finesse reached with the 200 μm fiber was 215 at a waist size of 150 μm and at an angle of 33.9 mrad. The reflection and transmission profiles, shown in Figure 23b., show a higher transmission at a 200 μm waist, and a corresponding lower reflection in this region. The rest of the profile shows that the reflection is higher in the mid-angle regions. The transmission at the mode-matched waist of 200 μm is exceeded at lower angles of larger waists, which remains around 3.5% from 400 μm to 1000 μm.

Beginning in the data for the 365 μm fiber, there are two regions of higher finesse. The mode-matched condition is not achieved with this fiber, but there is a higher region of finesse where the data approaches a waist of 190 μm. The other region of high finesse occurs at 913 μm, with a finesse of 178. At 913 μm, the beam waist is large and comes into the CFP nominally collimated. When the beam enters the CFP collimated, a region of high finesse emerges. Instead of focusing into the CFP such that the modes collapse, the collimated beam comes straight into the CFP, parallel to the optical axis, and then focuses such that all of the modes collapse, creating the same effect as the mode-matched condition. The transmission through the CFP decreases as the fiber diameters increase. The transmission at small angles hovers just below 2%, while at higher angles, the transmission remains around 1%. The reflection stays in the high 80% to low 90% region.

Again, with the 550 μm fiber, at a waist of 917 μm and an angle of 30.5 mrad, the finesse reaches 184. The mode-matched condition cannot be achieved with this large of a fiber, thus the only region of high finesse occurs when the light is collimated coming into the CFP. The transmission through the CFP is very low, ranging from 0.4% to 2.4%. The transmission is roughly constant through all angles and waists, with a 2% difference throughout the plot. The highest transmission occurs for large waists and small angles. The reflection ranges from 80% to 95%. There are areas of high reflection with large angles and large waists.

For verification of the percentage of the reflection and transmission of the CFP, consideration of the absorption of the mirrors in the CFP is necessary. The percentage of the reflection and transmission through the CFP consistently adds up from 80% to 90%, where the transmission is between, 0.5% to 5%, and the reflection ranges from 70% to 90%. The reflection and transmission coefficients were derived in the Theory section. Neglecting the phase, and adding in the absorption and scattering off of the mirrors, A, such that, R+T+A=1, and the reflection and transmission coefficients become:

$$T = (1 - \frac{A}{1 - R_m})^2, \tag{29}$$

where, R_m is the reflectivity of the mirrors, experimentally measured as 98.95%. The reflection coefficient, is:

$$R = R_m(\frac{A}{1 - R_m})^2. \tag{30}$$

Equations 29 and 30 can be manipulated to solve for the absorption coefficient, A. If the reflection and transmission that were experimentally determined are put into

these equations, the absorption coefficient is consistently 0.9%. Several of the experimental results of the reflection and transmission were input into the equations to solve for the absorption, with the results being consistent for both the reflection and the transmission. The measured value of the absorption and scattering off of the mirrors was determined to be 0.9%, also. The measurement was taken by placing a detector after the mirror and determining how much less light was collected than when placing the detector directly in the laser light.

There is a great deal of absorption and scattering associated with the mirrors of the CFP, yielding a low transmission through the CFP; however, these mirrors are not sealed within the CFP. The front mirror that is adjustable particularly spends some time exposed to the air. Also, dust particles from the air may cause a substantial increase in scattering from the mirror surfaces. The reflection and transmission measurements taken from the CFP can be validated using experiment and theory.

The trend of the CFP is that the finesse falls off as the fiber diameters increase. The largest finesse and transmission through the CFP occurred for the 62.5 μm fiber, the smallest multimode fiber used. There is a more dramatic constrast in reflection and transmission at the mode-matched waist for smaller fibers, from the 62.5 μm fiber through the 200 μm fiber, after which, the reflection and transmission profiles do not exhibit great contrast between regions of high finesse and low finesse. There are regions of high finesse when the CFP is mode-matched to the incoming light at a waist of 190 μm and the number of modes into the CFP is decreased. There also appears to be another region of higher finesse at 915 μm, where the light comes into the CFP collimated.

Verification of Two Lens Experiment Using 1 cm CFP

The data taken in this section is to verify that another CFP also follows the trends seen in the 5 cm homemade CFP. The CFP used here is a Thorlabs 1 cm CFP. The mode-matched condition is determined. The Rayleigh range can be calculated from equation 18 to be 0.5 cm. The beam waist is calculated using a λ of 532 nm:

$$w_0 = \sqrt{\frac{\lambda z_0}{\pi}} = \sqrt{\frac{532nm * 0.5cm}{\pi}} = 29 \tag{31}$$

The $1/e^2$ half-width is 29 μm, making the $1/e^2$ full-width 58 μm. Using the same V parameter calculated in equation 21, the fiber waist is again 44 μm, making the magnification factor, 58 μm/44 μm, or roughly 1.

The results of taking data with only the 62.5 μm fiber are shown in Figure 26. As predicted, there is a high finesse region where the mode-matched condition is satisfied at a waist of 94 μm and at an angle of 33.9 mrad. The highest finesse is 304. There is also high finesse at smaller angles, which averages a finesse of about 250.

Single Lens Experiment

The single lens experiment was conducted to capture all of the light from the multimode fiber and to vary the waist and the angle simultaneously. The setup for the experiment is shown in Figure 27. The setup for the single lens experiment is the same as the setup of the two lens experiment, with the exception of there being no collimating lens and no iris. The light is launched from a frequency stablized HeNe into a fiber. The light travels approximately 25 mm into a 25 mm focal length lens. All of the light is gathered by this lens. The light is then steered into the CFP by two steering mirrors. The light is brought to focus at the center of the cavity. To ensure everything is properly aligned, the second steering mirror, the cavity, and the

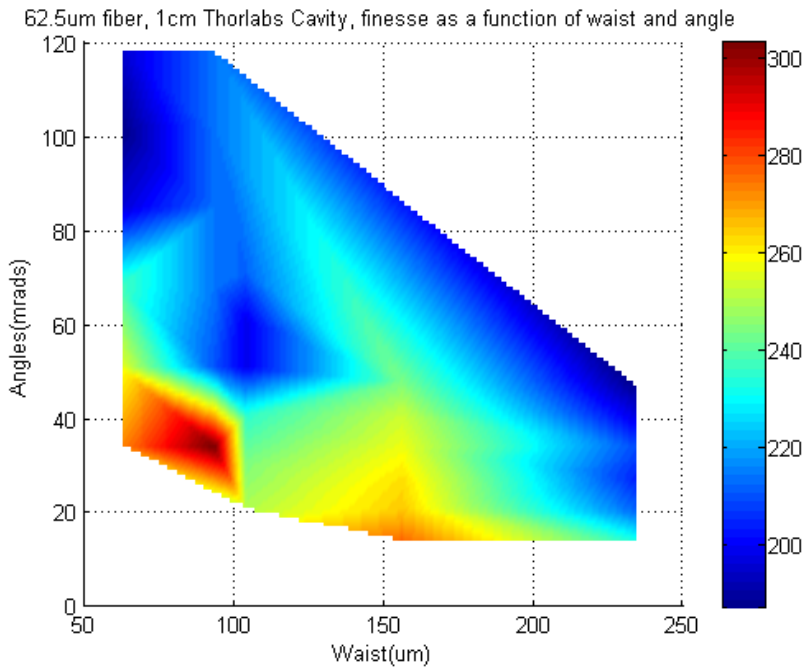

Figure 26: The finesse as a function of waist and angle for the Thorlabs 1 cm CFP.

detector are on a sliding rail, as shown on the right in Figure 27. The focusing lens is attached to a three-axis translation stage with a resolution of 0.001 inches, to make small adjustments. A flipper mirror was placed immediately before the CFP to find the focus of the beam and nominally place it at the center of the CFP.

Finesse measurements were taken for the single lens experiment. For the 5 cm CFP, the fibers used were the single mode, the 62.5 μm, the 100 μm, the 200 μm, the 365 μm, and the 550 μm. For the 1 cm cavity, the single mode, the 62.5 μm, the 100 μm, and the 200 μm fibers were used. The aperture of the 1 cm cavity was very small. The waist entering the cavity for fibers larger than 200 μm was clipped at the entrace to the cavity. For each fiber, finesse measurements were taken in 4 cm increments from a distance of 38 cm to 70 cm in front of the focusing lens to the center of the CFP. The focus was adjusted to remain at the center of the CFP at

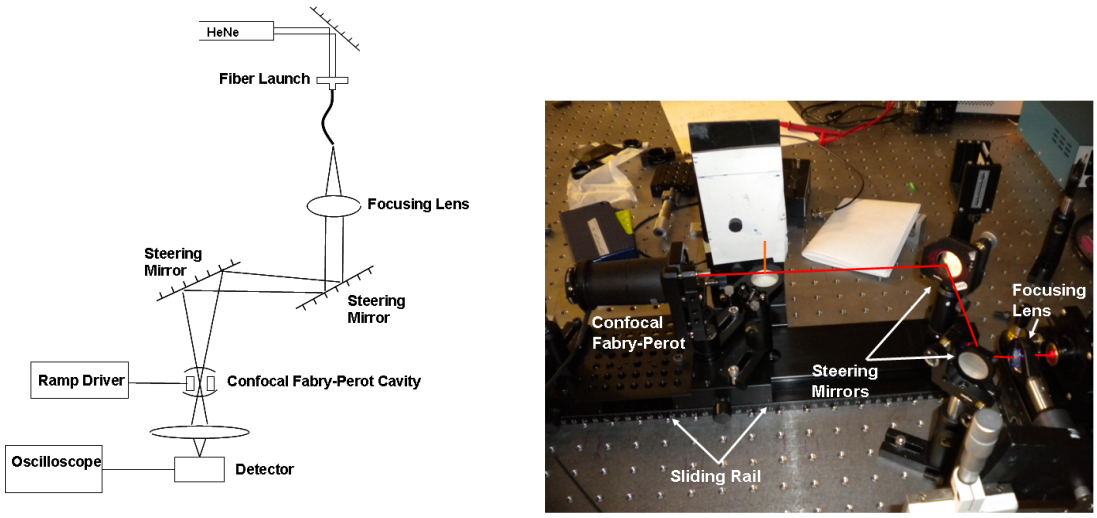

Figure 27: The schematic diagram of the single lens experimental setup is shown on the left, while the actual single lens experiment is shown on the right.

each distance by moving the focus of the focusing lens. The Thorlabs 5 cm and 1 cm CFP were used in this experiment.

Results of the Single Lens Experiment

The results of the experiment for both the 1 cm and 5 cm cavity are shown in Figures 28 and 29. For each fiber, the finesse largely stayed the same as a function of distance from the lens. The waist-angle product is the product between the beam diameter in the center of the cavity and the full-angle that the light is entering the cavity. The product stays the same as the cavity is moved because as the CFP moves further from the lens, the angle decreases, but the waist becomes larger, and likewise, when the CFP is closer to the lens, the waist is smaller, but the angle is larger. The product of the two quantities stays the same as the CFP is moved along the rail. The trend of the CFP is that the finesse is the same as the waist-angle product is maintained. An advantage to this attribute is if the CFP is setup initially in a certain

position for a system, but that position is found to be inconvenient, the CFP can be moved, with minor adjustments to the distance the lens moves and the finesse will remain the same.

The second set of plots in Figure 29 shows the finesse as a function of the waist-angle product. To make this plot, the data from Figure 28 were used. The points for each waist-angle product were fit to a line. The slope for the line was generally very near zero. The standard deviation of the line was accounted for in the error shown in Figure 29. Variation of the standard deviation from the average finesse for the fibers in the 5 cm cavity averaged 10.1%, with the range extending from 9.2% to 11.3%. The standard deviation of the fibers in the 1 cm cavity averaged 10.9%, with the range extending from 8.8% to 13.2%. The finesse could then be plotted as a function of the waist-angle product.

For the 5 cm Thorlabs CFP, the finesse falls off rapidly from the single mode fiber to the 100 μm fiber. The fall off continues from the 100 μm fiber to the 200 μm fiber, but not as drastically. The finesse levels off as a function of waist-angle product from the 200 μm fiber on. The total fall off finesse from the single mode fiber to the 550 μm fiber is roughly a factor of 3.5. The final finesse of the 550 μm fiber is 87. For the 1 cm Thorlabs CFP, the finesse does not drop off as quickly as the 5 cm cavity. The finesse is still dropping off at the 200 μm fiber, but ends at 240, falling by a factor of only 1.5 from the single mode fiber.

Summary of Experiment

A CFP cavity was built, aligned, and characterized. The characterization of the CFP included two experiments. The two lens experiment gathered information on the transmission, reflection, absorption, and finesse of the CFP in order to determine

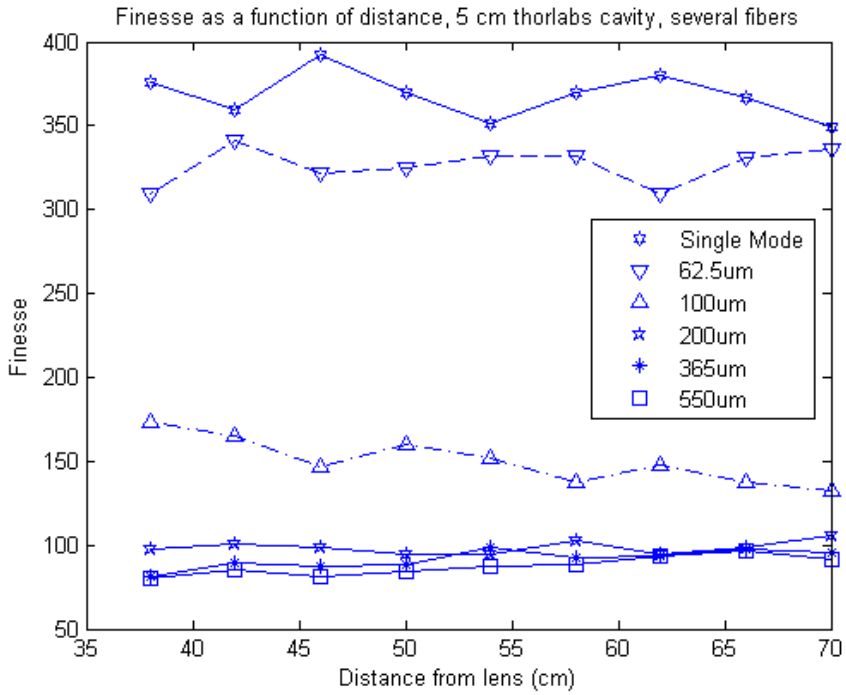

a.

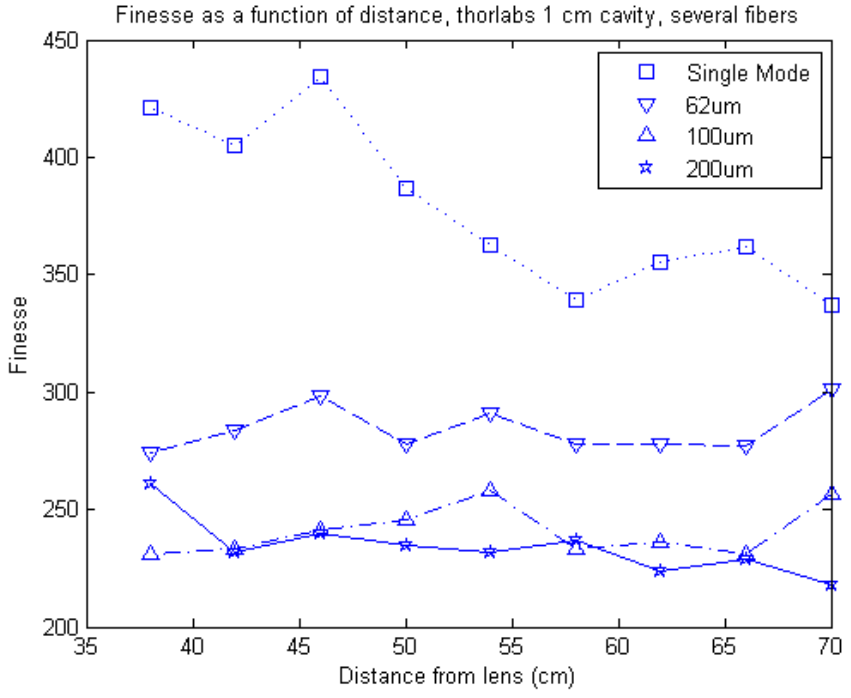

b.

Figure 28: The results of the single lens experiment for the 5 cm (a) and 1 cm (b) CFP of the finesse of the CFP as a function of the distance between the focusing lens and the center of the cavity for several different fibers, indicated in the legend.

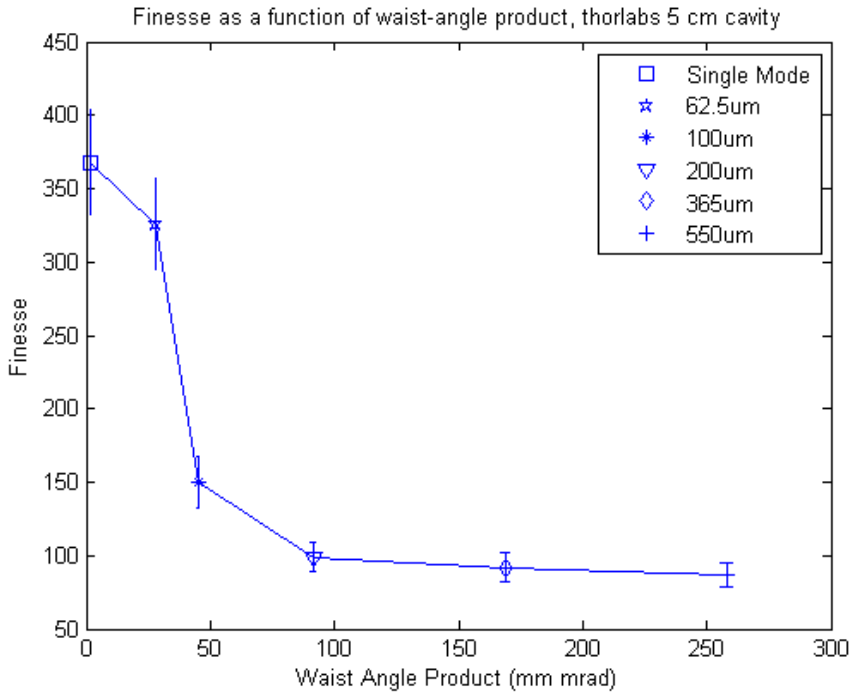

a.

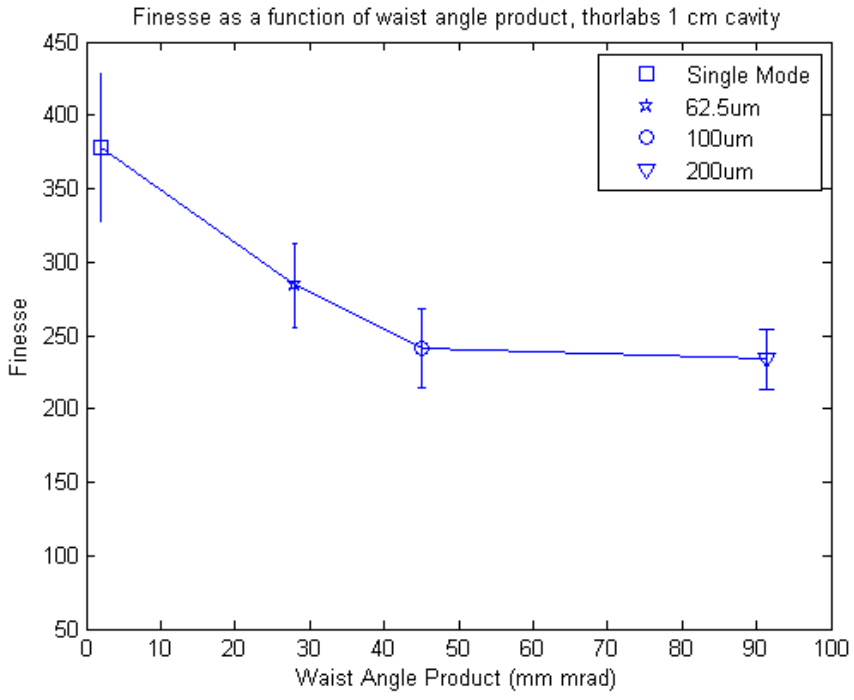

b.

Figure 29: The results of the single lens experiment for the 5 cm (a) and 1 cm (b) CFP of the finesse of the CFP as a function of the waist-angle product for several fibers, which are indicated in the legend.

the optimal configuration for the CFP in terms of high transmission and finesse, and low reflection. The two lens experiment showed that when the CFP is mode-matched or collimated upon entry into the cavity, there is high transmission and finesse. The single lens experiment determined the finesse as a function of the waist-angle product. It was determined that initially the finesse drops off substantially with waist-angle product, but levels off at a certain waist-angle product, keeping a constant finesse thereafter. In the next chapter, the results of these experiments are further analyzed in terms of known behavior of CFP cavities.

ANALYSIS

To obtain high finesse of the CFP, experimentally it was found that either mode-matching or collimating the light into the CFP was ideal. With mode-matching, the light focuses in the center of the cavity, where all of the higher-order modes collapse to form a single symmetric peak with high finesse. By collimating the light, the beam travels through the CFP first parallel to the optical axis, and then focuses at the foci of the two mirrors, but the same effect as mode-matching occurs, all of the modes collapse into a focus at the center of the CFP. By limiting the number of modes coming into the CFP from the fiber, by stopping down an iris, it is possible to increase the finesse. Trends observed in the CFP were that as the fiber diameter increases, typically the finesse decreases, as in the two lens experiment. Another trend is that the finesse of a CFP will remain constant with a constant waist-angle product. The finesse decreases with waist-angle product initially, but eventually levels off for larger fibers with larger waist-angle products.

Comparison of Experiment to Model

The model was run with multiple passes, up to 400, for waists up to 200 μm in diameter. A single pass model was run with waists up to 1 mm. The difference between a single pass and several hundred passes through the cavity was only a few milliradians. Nominally, the larger waists can be compared to the single pass model with a good degree of confidence.

There were consistent trends between the experiment and the model. First considered is the multipass model with waists up to 200 μm. The angles accepted into the CFP determined by the model went up to a full-angle of 115 mrad. All of the

measurements taken experimentally were at 118 mrad or below. The highest finesses occurred at angles far below 115 mrad, ranging from 10 to 40 mrad. The mode-matched condition, where there was a region of high finesse, occurred at 200 μm. This result is consistent with the model.

The model predicted for large waists that there would be only a narrow range of accepted angles in which a resonance would occur, this was not seen in actuality. Experimentally larger waists performed well, which indicates that the higher-order structure of the beam worked in favor of higher finesse at lower angles, or that the model was less capable of predicting the behavior of the CFP at larger waists. Another possibility is that the CFP can accept out-of-phase conditions extending beyond the tolerance of 63 mrad. This seems unlikely because the larger waist curves drop off substantially, as seen in Figure 10, indicating that a much larger tolerance of unphase-matched light would have to be accepted. The possibility of the model not being able to predict the behavior of larger waists is the most likely explanation, as the multimode nature of the light at a large waist is probably the most difficult configuration to accurately model. The model was only a ray trace and did not account for the multimode structure of the beam.

The waist-angle product generated from the model did not incorporate a large range of waist-angle products, the range was 0.79 mm mrad to 22.9 mm mrad. The experimental waist-angle product has a far wider range, from 2 mm mrad to 258 mm mrad. The smallest waist-angle products for the experiment and model correspond to the single mode fiber. The model predicts where the best finesse experimentally is achieved. The finesse remains above 300 from 2 mm mrad to 28 mm mrad in the experiment.

Comparison to Gaussian Beam Theory and Mode-Matching

The mode-matching condition calculated in the Theory section indicates that the waist size of the mode-matched CFP would be 142 μm for the 5 cm CFP and 58 μm for the 1 cm CFP. Experimentally the mode-matched waist of the 5 cm CFP was around 180 μm and the mode-matched waist of the 1 cm cavity was around 95 μm. The V parameter, which takes into account the modes within the fiber, calculated in equation 23, did predict the correct ratio of the focal lengths to obtain the mode-matched condition for the 5 cm and 1 cm CFP with the 62.5 μm fiber. The higher-order mode structure of the beam increases the size of the mode-matched waist.

Munnerlyn and Balliett [4] proposed that while mode-matching is not necessary, it does increase the transmission through the CFP by a factor of two. This result was found to be experimentally verified. The 62.5 μm fiber, when mode-matched into the CFP produced a transmission up to 9.8%, while the next highest transmission was 4.5% for the 100 μm fiber. The increase was slightly over a factor of two, which was exactly predicted by Munnerlyn and Balliett [4].

Comparison to Theory, Finesse Considerations

The theoretical finesse determined in the Theory section can be compared to the experimental data taken from the single lens experiment. The theoretical finesse is shown in Figure 5 and the experimental data for this comparison is shown in Figure 29. The radius of the beam at the front of the CFP can be extrapolated from the waist-angle product. The results of this are shown in Figure 30.

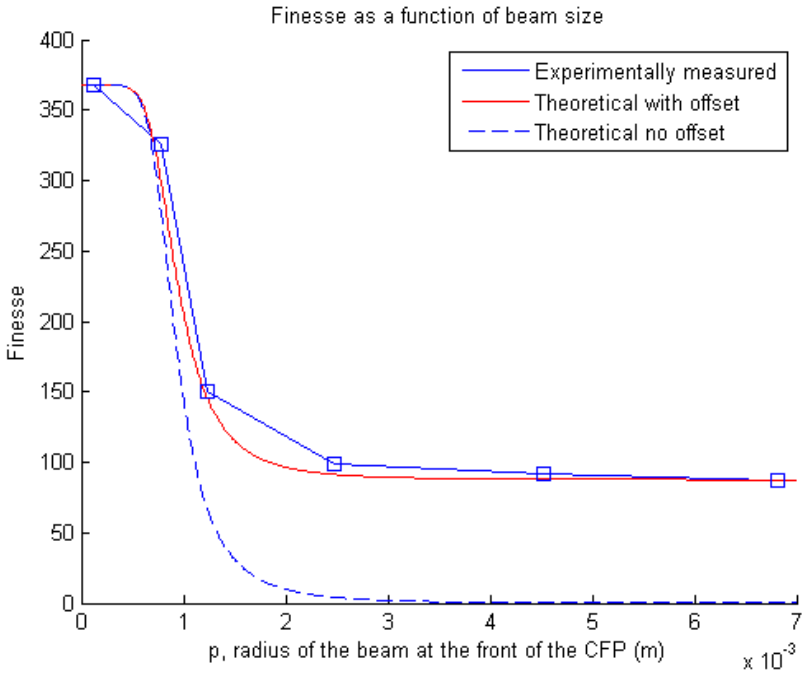

Figure 30: The comparison of the theoretical finesse, including the effect of spherical aberration, to the experimentally determined finesse as a function of the radius of the beam waist at the entrance to the cavity. The experimental results presented are from the 5 cm Thorlabs CFP. The theory is shown with no offset, akin to Figure 5, and also the theoretical result with an offset built in to better match the experimental data.

The finesse of the theoretical prediction falls rapidly to zero. Assuming that this represents the most extreme effects of spherical aberration and a large beam waist that is equal in size to the mirror radius, it is more realistic to introduce a factor that predicts the degree to which spherical aberration influences the finesse. A factor can be added to equation 11, which yields a total finesse of:

$$\mathcal{F}_{tot} = [(\frac{1-R^2}{\pi R})^2 + [(\frac{\rho^4}{2\lambda R_c^3})\frac{1}{1+(\rho/R_o)^4}]^2]^{-1/2}, \tag{32}$$

where R_o adjusts for the amount of spherical aberration present in a particular system. In this instance R_o is on the order of 1 mm. The theory predicts a slightly steeper fall off in finesse than the experimental data. Both the theory and the experiment demonstrate a constant finesse when the radius of the beam is roughly 2 mm in radius. The constant finesse approached by the theory is zero, while the finesse for the experiment is 90. The correction factor introduced in equation 32 better predicts the constant finesse that is approached by the experimental data. There is not a sound theoretical explanation yet realized for the reason why the finesse levels off at such a high finesse experimentally.

Comparison of the Experiments

Directly, it is difficult to compare the two experiments conducted; however, there are qualitative conclusions that can be drawn. The main difference between the two experiments was that the two lens experiment excluded mode structure of the fibers into the CFP, while the single lens experiment did not. Also, the waist-angle products in the two experiments did not overlap. The single lens experiment achieved much larger waist-angle products than the two lens experiment. Despite the differences, the general trends of finesse can be compared. For the two lens experiment in the mode-matched or collimated condition high finesse was achieved, but in other configurations

the CFP saw lower finesses. The outer regions of the interpolated plot for the 62.5 μm data, shown in Figure 21, had a finesse of above 200. Where for the 100 um fiber, the finesse dropped to around 150 in the regions outside of the mode-matched condition. The 200 μm fiber saw finesses of slightly over 100 and the 365 μm and 550 μm fiber saw finesses hovering around 100. The single lens experiment collects data for one point, rather than interpolating over a vast number of waist-angle products as seen in the two lens experiment. The single lens data showed the single mode fiber and the 62.5 μm fiber with very high finesses, well over 300. The 100 μm fiber had a finesse of 150. The remaining fibers of 200 μm, 365 μm, and 550 μm had a finesse hovering around 100. While the single lens data showed finesses that were slightly higher for the smaller fibers than the two lens experiment, a similar leveling off of the finesse occurred at a certain fiber diameter and waist-angle product. This trend of both experiments demonstrates that at a certain threshold the fiber diameter and the waist-angle product are irrelevant, and a consistent finesse can be achieved. The threshold discovered here was that beyond a fiber diameter of 200 μm and a waist-angle product of 100 mm mrad, the finesse remained nominally constant. While the theory does not exactly predict this trend, this trend is seen in both the single lens and two lens experiment. The trend is observed in the machined 5 cm CFP, as well as the Thorlabs 1 cm and 5 cm CFP.

The most promising result of the experiments conducted was that even for the largest diameter multimode fibers, while preserving all of the mode structure from the fiber, the finesse remained on the order of 100. Overall, the experiment proved that CFP interferometers are useful, in that they maintain high finesse and transmission. Specifically, with mode-matched conditions it is possible to attain high transmission and finesse. Also, with collimated conditions the CFP achieves high transmission and finesse. With these experimental results, the CFP performs well enough to be used

in a lidar receiver. With the vast parameter space explored in terms of fibers, angles, and waist sizes, a CFP can be constructed to work in a variety of different receiver setups.

CONCLUSION

A CFP has been modeled, designed, built, and characterized. From this work it has been deduced that a CFP will work in the receiver of a lidar as a narrowband filter. There are many favorable attributes to using a CFP in a lidar receiver. It has experimentally and theoretically been determined that large waists and large incoming angles are accepted into the CFP. The configuration is stable and not as sensitive to alignment as a FPFP. Achieving the mode-matched waist in the center of the CFP or collimating the input light to the CFP is ideal. It is not difficult to achieve these two conditions, which yield high finesse and high transmission through the CFP.

Trends that are advantageous to using the CFP as a filter in the lidar receiver are that the finesse stays constant if the waist-angle product stays constant. This is useful because the distance between the fiber and the lens, and the lens and the center of the CFP can change and as long as the waist-angle product stays the same, the finesse will remain constant. Also, considering finesse as a function of the waist-angle product, the finesse initially drops substantially as the waist-angle product increases, but levels off for large waist-angle products, ending at a finesse of around 90 using a fiber of 550 um in diameter. It has been shown that a CFP will be favorable as a narrowband filter in a lidar receiver, possessing several appealing characteristics over the current techniques of filtering signals in a lidar receiver.

Future Work

With the vast parameter space explored within this thesis, a CFP can be designed to be used in a specific lidar receiver. The main consideration of building a CFP is

the linewidth of the filter desired. This parameter can be changed by changing the length of the CFP, which implies choosing mirrors with the correct radii of curvature to establish the specific FSR necessary. Mirrors can be built with substantially lower absorption to achieve higher transmissions than those used in the experiments considered. The finesse and transmission of any CFP can be predicted based on the measurements taken within this thesis.

Thus far, the CFP has been incorporated into the HSRL, which is starting to take data as of the writing of this thesis. The results of the CFP used in this application will determine the success of the CFP to those in the lidar community.

REFERENCES

[1] J. Vaughn, "The fabry-perot interferometer: History, theory, practice and applications," IOP Publishing Ltd, Bristol, England and Philadelphia, PA, USA, 1989.

[2] K. Kerner, S. Rochester, V. Yashchuk, and D. Budker, "Variable free spectral range spherical mirror fabry-perot interferometer," *eprint arXiv:physics/0306144*, pp. 1–11, 2003.

[3] M. Hercher, "The spherical mirror fabry-perot," *Applied Optics*, vol. 7, pp. 951–966, 1968.

[4] C. Munnerlyn and J. Balliett, "Alignment requirements for mode matching in a confocal fabry-perot interferometer," *Applied Optics*, vol. 9, no. 11, pp. 2535–2538, 1970.

[5] G. Gary, C. Pietraszewski, E. West, and T. Dines, "Solar confocal interferometers for sub-picometer-resolution spectral filters," *Astronomy and Astrophysics*, vol. 467, pp. 375–383, 2007.

[6] "Interference filters," *CVI Melles Griot Catalog, http://www.mellesgriot.com/glossary/wordlist/glossarydetails.asp?wID=338*, 2009.

[7] S. Shipley, D. Tracy, E. Eloranta, and et. al., "High spectral resolution lidar to measure optical scattering properties of atmospheric aerosols 1: Theory and instrumentation," *Applied Optics*, vol. 22, pp. 3716–3724, 1983.

[8] D. Winker, J. Pelon, and M. McCormick, "The calipso mission: Spaceborne lidar for observation of aerosols and clouds," *Proceedings of SPIE Lidar Remote Sensing for Industry and Environment Monitoring III*, 2003.

[9] R. Sica, S. Sargoytchev, P. Argall, and et. al., "Lidar measurements taken with a large-aperture liquid mirror 1. rayleigh-scatter system," *Applied Optics*, vol. 34, no. 30, pp. 6925–6936, 1995.

[10] E. Eloranta and edited by Claus Weitkamp, "High spectral resolution lidar in lidar: Range-resolved optical remote sensing of the atmosphere," Springer Science, New York, NY, USA, 2005.

[11] J. Hair, L. Caldwell, D. Krueger, and C. She, "High spectral-resolution lidar with iodine-vapor filters: Measurements of atmospheric-state and aerosol profiles," *Applied Optics*, vol. 40, pp. 5280–5294, 2001.

[12] R. E. Fischer and B. Tadic-Galeb, "Optical system design," McGraw Hill, New York, NY, USA, 2000.

[13] J. Johnson, "A high resolution scanning confocal interferometer," *Applied Optics*, vol. 7, no. 6, pp. 1061–1072, 1968.

[14] "Scanning fabry-perot interferometers, derivation of the finesse," *Thorlabs Catalog*, vol. 19, pp. 648–652, 2007.

[15] G. Holah and S. Smith, "Multi-element mesh interference filters for the infrared," *Journal of Physics D: Applied Physics*, pp. 496–505, 1972.

[16] "Liquid crystal filled fabry-perot filter," *Meadowlark Optics Application Note*, pp. 1–4, 2005.

[17] K. Repasky, L. Watson, and J. Carlsten, "High finesse interferometers," *Applied Optics*, vol. 34, pp. 2615–2618, 1995.

[18] G. P. Agrawal, "Lightwave technology: Components and devices," John Wiley and Sons, Inc., Hoboken, NJ, USA, 2004.

[19] B. Saleh and M. Teich, "Fundamentals of photonics," John Wiley and Sons, Inc., New York, NY, USA, 1991.

APPENDIX A

MATLAB CODE FOR MODELING

Spherical Mirror, Off-Axis Small Angle Program

```
function [pathdifference, dtotal]=spherical_offaxis_smangles_n(m0, R, N, y0)
%Program to calculate the optical path length of a confocal cavity with
%   spherical mirrors and small angles off axis
%Kerry Neal 07/2008

%m0 = input slope of the initial ray, enters into the center of the cavity
%   can be an array, example m0=1e-3:0.68e-4:0.2047;
%R = Radius of curvature of the mirrors in centimeters
%y0 = off-axis starting position of the light
%N = number of passes through the cavity, equal to finesse
x0=0.0;
delta=0.0;
dtotal=[];
deg=180./pi*(atan(m0));

for i=1:N

    %Initial angle
    theta0=atan(m0);

    % 1) Propagate to right mirror and find intersection (x1, y1) on
    % mirror
    a=1+(m0).^2;
    b=R+2.*delta+2.*m0.*(y0-m0.*x0);
    c=(y0-m0.*x0).^2-(3*R^2)./4+(R*delta+(delta)^2);
    x1=(-b+sqrt(b.^2-4.*a.*c))./(2.*a);
    y1=m0.*(x1-x0)+y0;

    %distance d1 traveled from (x0, y0) to (x1, y1)
    d1=sqrt((x1-x0).^2+(y1-y0).^2);

    % 2) Slope of surface of right mirror at (x1, y1)
    slope=-(x1+R/2+delta)./(sqrt(R.^2-(x1+R/2+delta).^2));
    normal=-1./slope;
    thetan=atan(normal);
    %slope of reflection from mirror
    theta1=2.*thetan-theta0;
    m1=tan(theta1);

    % 3) Propagate to left mirror
    a=1+(m1).^2;
    b=-R+2.*m1.*(y1-m1.*x1);
    c=(y1-m1.*x1).^2-(3*R^2)./4;
    x2=(-b-sqrt(b.^2-4.*a.*c))./(2.*a);
    y2=(m1.*(x2-x1)+y1);

    %distance traveled
    d2=sqrt((x2-x1).^2+(y2-y1).^2);
```

```
% 4) Slope at left mirror
slope=(x2-R/2)./(sqrt(R.^2-(x2-R/2).^2)+1.*10^-13);

%find slope of normal to mirror
normal=-1./slope;
thetan=atan(normal);
%find slope of reflection
theta2=2.*thetan-theta1;
m2=tan(theta2);


% 5) Propagate to right mirror

a=1+(m2).^2;
b=R+2.*delta+2*m2.*(y2-m2.*x2);
c=(y2-m2.*x2).^2-(3*R^2)./(4+(R*delta+(delta)^2));
x3=(-b+sqrt(b.^2-4.*a.*c))./(2.*a);
y3=m2.*(x3-x2)+y2;


%find distance traveled
d3=sqrt((x3-x2).^2+(y3-y2).^2);


% 6) find slope at right mirror
slope=(x3+R/2+delta)./(sqrt((R.^2-(x3+R/2+delta).^2)));
%find slope of normal to mirror
normal=-1./slope;
thetan=atan(normal);
%find slope of reflection
theta3=2.*thetan-theta2;
m3=tan(theta3);

% 7) Propagate to left mirror
a=1+(m3).^2;
b=-R+2*m3.*(y3-m3.*x3);
c=(y3-m3.*x3).^2-(3*R^2)./4;
x4=(-b-sqrt(b.^2-4.*a.*c))./(2.*a);
y4=m3.*(x4-x3)+y3;

%find distance traveled
d4=sqrt((x4-x3).^2+(y4-y3).^2);

% 8) find slope at left mirror
slope=-(x4-R/2)./(sqrt((R.^2-(x4-R/2).^2)));
normal=-1./slope;
thetan=atan(normal);
theta4=2.*thetan-theta3;
m4=tan(theta4);
```

```
    % 9) Propagate to left mirror
    x5=0;
    y5=m4.*(x5-x4)+y4;

    %distance traveled
    d5=sqrt((x5-x4).^2+(y5-y4).^2);

       dtotal(i,:)=d1+d2+d3+d4+d5;

    %pathdifference(i,:)=dtotal(i, :)-(N*4*R);


    %reset x0, y0, and m0 for next iteration
   x0=x5;
   y0=y5;
   m0=m4;
   j=i;
end
dtot=sum(dtotal,1);
pathdifference=dtot-(N*4*R);

plot(deg, pathdifference), xlabel('slope (degrees)'), ylabel('optical path difference (mm)')
```

Spherical Mirror, Off-Axis Large Angle Program

```
function [pathdifference, dtotal]=spherical_offaxis_lgangles_n(m0, R, N, y0)
%Program to calculate the optical path length of a confocal cavity with
%   spherical mirrors and large angles off axis
%Kerry Neal 07/2008

%m0 = input slope of the initial ray, enters into the center of the cavity
%   can be an array, example m0=1e-3:0.68e-4:0.2047;
%R = Radius of curvature of the mirrors in centimeters
%y0 = off-axis starting position of the light
%N = number of passes through the cavity, equal to finesse
x0=0.0;
delta=0.0;
dtotal=[];
deg=180./pi*(atan(m0));

for i=1:N
    %clear dtotal
    %Initial angle
    theta0=atan(m0);

    % 1) Propagate to right mirror and find intersection (x1, y1) on
```

```
% mirror
a=1+(m0).^2;
b=R+2.*delta+2.*m0.*(y0-m0.*x0);
c=(y0-m0.*x0).^2-(3*R^2)./4+(R*delta+(delta)^2);
x1=(-b+sqrt(b.^2-4.*a.*c))./(2.*a);
y1=m0.*(x1-x0)+y0;

%distance d1 traveled from (x0, y0) to (x1, y1)
d1=sqrt((x1-x0).^2+(y1-y0).^2);
%d1_r=d1*10^9
%d1_r=round(d1_r)
%d1_r=d1_r/10^9

% 2) Slope of surface of right mirror at (x1, y1)
slope=-(x1+R/2+delta)./(sqrt(R.^2-(x1+R/2+delta).^2));
normal=-1./slope;
thetan=atan(normal);
%slope of reflection from mirror
theta1=2.*thetan-theta0;
m1=tan(theta1);

% 3) Propagate to left mirror
a=1+(m1).^2;
b=-R+2.*m1.*(y1-m1.*x1);
c=(y1-m1.*x1).^2-(3*R^2)./4;
x2=(-b-sqrt(b.^2-4.*a.*c))./(2.*a);
y2=(m1.*(x2-x1)+y1);

%distance traveled
d2=sqrt((x2-x1).^2+(y2-y1).^2);

% 4) Slope at left mirror
slope=-(x2-R/2)./(sqrt(R.^2-(x2-R/2).^2)+1.*10^-13);

%find slope of normal to mirror
normal=-1./slope;
thetan=atan(normal);
%find slope of reflection
theta2=2.*thetan-theta1;
m2=tan(theta2);


% 5) Propagate to right mirror

a=1+(m2).^2;
b=R+2.*delta+2*m2.*(y2-m2.*x2);
c=(y2-m2.*x2).^2-(3*R^2)./(4+(R*delta+(delta)^2));
x3=(-b+sqrt(b.^2-4.*a.*c))./(2.*a);
y3=m2.*(x3-x2)+y2;
```

```
    %find distance traveled
    d3=sqrt((x3-x2).^2+(y3-y2).^2);

    % 6) find slope at right mirror
    slope=(x3+R/2+delta)./(sqrt((R.^2-(x3+R/2+delta).^2)));
    %find slope of normal to mirror
    normal=-1./slope;
    thetan=atan(normal);
    %find slope of reflection
    theta3=2.*thetan-theta2;
    m3=tan(theta3);

    % 7) Propagate to left mirror
      a=1+(m3).^2;
    b=-R+2*m3.*(y3-m3.*x3);
    c=(y3-m3.*x3).^2-(3*R^2)./4;
    x4=(-b-sqrt(b.^2-4.*a.*c))./(2.*a);
    y4=m3.*(x4-x3)+y3;

    %find distance traveled
    d4=sqrt((x4-x3).^2+(y4-y3).^2);

    % 8) find slope at left mirror
    slope=(x4-R/2)./(sqrt((R.^2-(x4-R/2).^2)));
    normal=-1./slope;
    thetan=atan(normal);
    theta4=2.*thetan-theta3;
    m4=tan(theta4);

    % 9) Propagate to left mirror
    x5=0;
    y5=m4.*(x5-x4)+y4;

    %distance traveled
    d5=sqrt((x5-x4).^2+(y5-y4).^2);

    dtotal(i,:)=d1+d2+d3+d4+d5;

    %pathdifference(i,:)=dtotal(i, :)-(N*4*R);


    %reset x0, y0, and m0 for next iteration
   x0=x5;
   y0=y5;
   m0=m4;
   j=i;
end
dtot=sum(dtotal,1);
pathdifference=dtot-(N*4*R);

plot(deg, pathdifference), xlabel('slope (degrees)'), ylabel('optical path difference (mm)')
```

Program to concatenate both spherical mirror cavity programs

```
function [concat]=sphere_family_n(m0, R, y0, N)
%Program to calculate the optical path length of a confocal cavity with
%   spherical mirrors, this program concatenates the two spherical programs
%   for large and small angles coming into the cavity
%Kerry Neal 07/2008

%m0 = input slope of the initial ray, enters into the center of the cavity
%   can be an array, example m0=1e-3:0.68e-4:0.2047;
%R = Radius of curvature of the mirrors in centimeters
%y0 = off-axis starting position of the light
%N = number of passes through the cavity, equal to finesse

close all
    deg=180./pi*(atan(m0));
[pathdif1, dtot1]=spherical_offaxis_lgangles_n(m0, R, N, y0);

[x, i]=min(pathdif1)

the_end=pathdif1(i+1:2996);

plot(the_end)

pathdif2=spherical_offaxis_smangles_n(m0, R, N, y0);
the_beg=pathdif2(1:i);

concat=[the_beg the_end];
figure
plot(concat)
figure
plot(deg, concat), xlabel('degrees'), ylabel('optical path difference (mm)')
y=6.33e-6*N;
hold on
plot(deg, y)
```

Parabolic Mirrors, Off-Axis Small Angle Program

```
function [pathdifference]=parabolasang_n(m0, R, p, N, y0)

%Program to calculate the optical path length of a confocal cavity with
%   parabolic mirrors.
```

```
%Kerry Neal 07/08/2008

%m0=input slope of the initial ray, enters into the center of the cavity
%   can be an array
%R = Radius of curvature of the mirrors
%N=number of passes through the cavity, equal to finesse
%p=distance from the focus to the vertex of the parabola

x0=0.0;
delta=0.0;
dtotal=[];
deg=180./pi*(atan(m0));

for i=1:N

    %Initial angle
    theta0=atan(m0);

    % 1) Propagate to right mirror and find intersection (x1, y1) on
    % mirror
    a=(m0).^2;
    b=2*m0.*y0-2*m0.^2*x0+4*p;
    c=(m0.*x0).^2-2*m0.*x0.*y0+y0.^2-4*p.^2;
    x1=(-b+sqrt(b.^2-4.*a.*c))./(2.*a);
    y1=m0.*(x1-x0)+y0;

    %distance d1 traveled from (x0, y0) to (x1, y1)
    d1=sqrt((x1-x0).^2+(y1-y0).^2);

    % 2) Slope of surface of right mirror at (x1, y1)
    slope=(-2*p)./(sqrt(-(4*p*(x1-p))));
    normal=-1./slope;
    thetan=atan(normal);
    %slope of reflection from mirror
    theta1=2.*thetan-theta0;
    m1=tan(theta1);

    % 3) Propagate to left mirror
    a=(m1).^2;
    b=2*m1.*y1-2*m1.^2.*x1-4*p;
    c=(m1.*x1).^2-2*m1.*x1.*y1+y1.^2-4.*p.^2;
    x2=(-b-sqrt(b.^2-4.*a.*c))./(2.*a);
    y2=m1.*(x2-x1)+y1;


    %distance traveled
    d2=sqrt((x2-x1).^2+(y2-y1).^2);

    % 4) Slope at left mirror
    slope=(-2*p)./(sqrt((4*p*(x2+p))));
    normal=-1./slope;
```

```
thetan=atan(normal);
%slope of reflection from mirror
theta2=2.*thetan-theta1;
m2=tan(theta2);

% 5) Propagate to right mirror
a=(m2).^2;
b=2*m2.*y2-2*m2.^2.*x2+4*p;
c=(m2.*x2).^2-2*m2.*x2.*y2+y2.^2-4*p^2;
x3=(-b+sqrt(b.^2-4.*a.*c))./(2.*a);
y3=m2.*(x3-x2)+y2;

%find distance traveled
d3=sqrt((x3-x2).^2+(y3-y2).^2)

% 6) find slope at right mirror
slope=(2*p)./(sqrt(-(4*p*(x3-p))));
normal=-1./slope;
thetan=atan(normal);
%slope of reflection from mirror
theta3=2.*thetan-theta2;
m3=tan(theta3);

% 7) Propagate to left mirror
 a=(m3).^2;
b=2*m3.*y3-2*m3.^2.*x3-4*p;
c=(m3.*x3).^2-2*m3.*x3.*y3+y3.^2-4*p^2;
x4=(-b-sqrt(b.^2-4.*a.*c))./(2.*a);
y4=m3.*(x4-x3)+y3;


%find distance traveled
d4=sqrt((x4-x3).^2+(y4-y3).^2);

% 8) find slope at left mirror
slope=(2*p)./(sqrt(4*p*(x4+p)));
normal=-1./slope;
thetan=atan(normal);
%slope of reflection from mirror
theta4=2.*thetan-theta3;
m4=tan(theta4);

% 9) Propagate to center of mirrors
x5=0;
y5=m4.*(x5-x4)+y4;

%distance traveled
d5=sqrt((x5-x4).^2+(y5-y4).^2);

dtotal=d1+d2+d3+d4+d5;
```

```
  pathdifference(i,:)=dtotal-(1*4*R);


    %reset x0, y0, and m0 for next iteration
    x0=x5;
    y0=y5;
    m0=m4;
    j=i;
end
figure()
plot(deg, pathdifference), xlabel('slope (degrees)'), ylabel('optical path length (mm)')
```

Parabolic Mirrors, Off-Axis Large Angle Program

```
function [pathdifference m0]=parabolalang_n(m0, R, p,N, y0)

%Program to calculate the optical path length of a confocal cavity with
%   parabolic mirrors.
%Kerry Neal 07/08/2008

%m0=input slope of the initial ray, enters into the center of the cavity
%   can be an array
%R = Radius of curvature of the mirrors
%N=number of passes through the cavity, equal to finesse
%p=distance from the focus to the vertex of the parabola

x0=0.0;
delta=0.0;
dtotal=[];
deg=180./pi*(atan(m0));

for i=1:N

    %Initial angle
    theta0=atan(m0);

    % 1) Propagate to right mirror and find intersection (x1, y1) on
    % mirror
    a=(m0).^2;
    b=2*m0.*y0-2*m0.^2*x0+4*p;
    c=(m0.*x0).^2-2*m0.*x0.*y0+y0.^2-4*p.^2;
    x1=(-b+sqrt(b.^2-4.*a.*c))./(2.*a);
    y1=m0.*(x1-x0)+y0;

    %distance d1 traveled from (x0, y0) to (x1, y1)
    d1=sqrt((x1-x0).^2+(y1-y0).^2);
```

```
% 2) Slope of surface of right mirror at (x1, y1)
slope=(-2*p)./(sqrt(-(4*p*(x1-p))));
normal=-1./slope;
thetan=atan(normal);
%slope of reflection from mirror
theta1=2.*thetan-theta0;
m1=tan(theta1);

% 3) Propagate to left mirror
a=(m1).^2;
b=2*m1.*y1-2*m1.^2.*x1-4*p;
c=(m1.*x1).^2-2*m1.*x1.*y1+y1.^2-4.*p.^2;
x2=(-b-sqrt(b.^2-4.*a.*c))./(2.*a);
y2=m1.*(x2-x1)+y1;


%distance traveled
d2=sqrt((x2-x1).^2+(y2-y1).^2);

% 4) Slope at left mirror
slope=(2*p)./(sqrt((4*p*(x2+p))));
normal=-1./slope;
thetan=atan(normal);
%slope of reflection from mirror
theta2=2.*thetan-theta1;
m2=tan(theta2);

% 5) Propagate to right mirror
a=(m2).^2;
b=2*m2.*y2-2*m2.^2.*x2+4*p;
c=(m2.*x2).^2-2*m2.*x2.*y2+y2.^2-4*p^2;
x3=(-b+sqrt(b.^2-4.*a.*c))./(2.*a);
y3=m2.*(x3-x2)+y2;

%find distance traveled
d3=sqrt((x3-x2).^2+(y3-y2).^2);

% 6) find slope at right mirror
slope=(2*p)./(sqrt(-(4*p*(x3-p))));
normal=-1./slope;
thetan=atan(normal);
%slope of reflection from mirror
theta3=2.*thetan-theta2;
m3=tan(theta3);

% 7) Propagate to left mirror
 a=(m3).^2;
b=2*m3.*y3-2*m3.^2.*x3-4*p;
c=(m3.*x3).^2-2*m3.*x3.*y3+y3.^2-4*p^2;
x4=(-b-sqrt(b.^2-4.*a.*c))./(2.*a)
```

```
    y4=m3.*(x4-x3)+y3;


    %find distance traveled
    d4=sqrt((x4-x3).^2+(y4-y3).^2);

    % 8) find slope at left mirror
    slope=(-2*p)./(sqrt(4*p*(x4+p)));
    normal=-1./slope;
    thetan=atan(normal);
    %slope of reflection from mirror
    theta4=2.*thetan-theta3;
    m4=tan(theta4);

    % 9) Propagate to center of mirrors
    x5=0;
    y5=m4.*(x5-x4)+y4;

    %distance traveled
    d5=sqrt((x5-x4).^2+(y5-y4).^2);

    dtotal=d1+d2+d3+d4+d5;

  pathdifference(i,:)=dtotal-(1*4*R);


    %reset x0, y0, and m0 for next iteration
    x0=x5;
    y0=y5;
    m0=m4;
    j=i;
end


figure()
plot(deg, pathdifference), xlabel('slope (degrees)'), ylabel('optical path length (mm)')
```

Program that concatenates the small and large angle parabolic mirror cavity programs

```
function [concat]=parabola_family_n(m0, R, p, N, y0)
%Program to calculate the optical path length of a confocal cavity with
%   parabolic mirrors, this program concatenates the two parabolic programs
%   for large and small angles coming into the cavity.
%Kerry Neal 07/2008

%m0=input slope of the initial ray, enters into the center of the cavity
%   can be an array
```

```
%R = Radius of curvature of the mirrors
%N=number of passes through the cavity, equal to finesse
%p=distance from the focus to the vertex of the parabola

[pathdif1 slope]=parabolalang_n(m0, R, p, N, y0);

[x,i]=min(slope);

the_end_cut=pathdif1(N,:);
the_end=the_end_cut(i+1:2996);

plot(the_end)

pathdif2=parabolasang_n(m0, R, p, N, y0);
the_beg_cut=pathdif2(N,:);

the_beg=the_beg_cut(1:i);

concat=[the_beg the_end];

deg=180./pi*(atan(m0));
plot(deg, concat), xlabel('degrees'), ylabel('optical path difference (mm)')
```